16th ICAAR LISBOA 2020-2022

16th International Conference on
Alkali-Aggregate Reaction in Concrete
Lisboa | LNEC | Portugal | 31 May - 2 June 2022

http://icaar2020-2022.lnec.pt

Alkali-silica reaction in concrete - Physical and chemical effects

Benoit Fournier[(1)], Samy-Joseph Essalik[(2)], Mathieu Champagne[(3)], Anthony Allard[(4)], Benoit Bissonnette[(5)]

(1) *Département de géologie et de génie géologique, Université Laval, Québec, Canada, benoit.fournier@ggl.ulaval.ca*

(2) *Département de génie civil et de génie des eaux, Université Laval, Québec, Canada,* samy-joseph.essalik.1@ulaval.ca

(3) *Département de géologie et de génie géologique, Université Laval, Québec, Canada, mathieu.champagne.8@ulaval.ca*

(4) *Englobe, Expertise – Material engineering, Québec, Canada, Anthony.Allard@englobecorp.com*

(5) *Département de génie civil et de génie des eaux, Université Laval, Québec, Canada, Benoit.Bissonnette@gci.ulaval.ca*

Abstract

Various instable forms of silica present in some fine or coarse concrete aggregates can react with the alkali hydroxides from the pore solution to form a hydrophilic secondary reaction product that generate internal stresses within the reacting particles and the surrounding cement paste, eventually causing distress in the affected element or structure. This phenomenon, known as alkali-silica reaction, is one of the main pathologies affecting the service life of the concrete infrastructure worldwide. This papers reviews some of the main physical and chemical effects of ASR on concrete structures. It focuses on the development of expansion, a physical symptom of ASR which is the most widely used in laboratory testing for determining potential alkali-reactivity of concrete aggregates, as well as for the assessment of various preventive or mitigation measures against this pathology. The influence of internal and external restraints on the development of expansion and cracking due to ASR is also reviewed, based upon laboratory investigations and case studies. Finally, specific considerations pertaining to the roles played by two critical parameters for the development of ASR expansion and cracking, namely moisture and the concrete alkali content, are discussed.

***Keywords**: ASR, Expansion, Cracking, Concrete Alkali content, Alkali contribution from aggregates*

1. INTRODUCTION

1.1 Opening remarks

Alkali-silica reaction (ASR) is part of the main pathologies affecting concrete durability worldwide. ASR damage results from the swelling of secondary reaction products within fine/coarse reactive aggregate particles and the surrounding cement paste. Numerous publications identified the critical parameters for ASR to develop and be maintained in concrete as 1) the presence of reactive siliceous phase within the coarse/fine aggregates, 2) the availability of moisture and 3) high alkali concentration resulting in high pH in the concrete pore solution [1,2].

Expansion and *cracking* are the most common physical effects of this concrete pathology. The extent of ASR expansion and resulting cracking in structures such as bridges, dams, buildings, pavements, is influenced by numerous factors including the concrete mixture characteristics (e.g. reactive rock type and proportion, cementitious materials and concrete alkali contents, w/cm, etc.), “environmental” conditions (e.g. humidity, temperature, exposure to sun, wind, etc.), and restraints. Variations in the above factors from one location to another result in differential expansion/movements between adjacent elements/components, closure, overstress and spalling at joints, operational issues, etc. [1-3].

This paper presents some thoughts and examples from laboratory and field investigations relating to physical and chemical effects of ASR. For the latter, focus will be given to the potential alkali contribution from aggregates in concrete.

1.2 Test methods for diagnosis and prognosis

Data are reported in this paper from the use of different test methods for condition assessment (*diagnosis*) and determination of potential future damage generation (*prognosis*) in concrete affected by ASR. The *Stiffness Damage Test* (SDT) is a cyclical compression test where a concrete cylinder/core undergoes five cycles of loading-unloading at a fixed rate of 0,1 MPa/sec and using a maximum load corresponding to 40% of the compressive strength of the undamaged concrete [4]. The SDT outputs commonly used for damage assessment are the *Stiffness Damage Index* (SDI), which corresponds to the ratio between the dissipated energy and the total energy used during the test (five cycles) and the modulus of elasticity (E_c) averaged from the 2nd and 3rd loading cycles [5].

The *Damage Rating Index* (DRI) method consists in a petrographic analysis on polished concrete section to quantify the occurrence of petrographic features of ASR. A grid of 1 x 1 cm^2 is drawn on the surface and deterioration features are counted in each square (minimum 200 cm^2) with a stereobinocular microscope at 15× magnification. The sum of those counts is then multiplied by selected weighing factors [6] and the total, which is normalized for a surface area of 100 cm^2, represents the *DRI number*. Procedures for spatial damage characterization using DRI data were recently proposed [7-8].

The *Cracking Index* (CI) method involves the measurement and summation of crack widths along a set of lines drawn in the vertical and horizontal directions on the surface of the concrete element investigated [9]. The results are expressed in mm/m.

The *hot-water alkali extraction* (HWE) method uses a 10 g powder sample (particles $<$ 150 µm) from a ground concrete specimen, that is mixed in 80 mL of distilled water and boiled for ten minutes. The solution is then filtered, completed to 100 mL and analyzed for its alkali content using appropriate means. The results are expressed in kg of alkalis per m^3 of concrete, using a measure (or a reliable estimate) of the concrete density [10]. The *cold-water extraction* (CWE) uses powder sample (particles $<$ 80 µm) mixed with deionized water (liquid-to-solid ratio of 1) for 5 min at room temperature and the suspension filtered to determine the Na and K contents of the filtrate [11].

2. ALKALI-SILICA REACTION - PHYSICAL EFFECTS

2.1 Expansion due to ASR

2.1.1 Free expansion under accelerated laboratory conditions

Expansion is the most commonly used physical parameter in laboratory testing for evaluating the potential reactivity of concrete aggregates and preventive measures against ASR. Since the 1940's, numerous accelerated ASR expansion tests on mortar/concrete have been developed that involve increased alkali levels (boosting alkalis in the original mixture or immersion in alkaline/salt solutions, e.g. NaOH, KOH, NaCl) and/or storage under high relative humidity (RH), temperature (e.g. 38, 50, 60, 80°C) and pressure conditions. The threshold alkali and RH values above which expansion beyond the accepted test limit occurs depend on the nature of the reactive material/aggregate [1,12] (Figure 2.1A) and the testing temperature [13]. Concrete specimens stored at 100% RH display faster onset of expansion at higher temperatures (e.g. 60°C; Figure 2.1B), but expansion may level off rapidly because of faster alkali leaching [14]. The extent of expansion of test prisms stored in alkaline solutions increases with temperature (Figure 2.1B); however, it also varies according to the aggregate particle and prism sizes, as it affects the amount of secondary reaction products oozing out of the specimens in the immersion solution [15-17].

Dedicated outdoor exposure sites have been used by a number of investigators over the past few decades for validating the results of laboratory testing [18]. Figure 2.2 compares the expansive behaviour of ten reactive aggregates in the Accelerated Mortar Bar Test (AMBT), Concrete Prism Test (CPT) and field test blocks ageing in outdoor exposure conditions. All reactive aggregates show a steadily increasing expansion process within the 14-day testing period in the AMBT, the difference being essentially the slope of the expansion curves (Figure 2.2A). Most aggregates display a "S-shape" expansion curve over the 104-week concrete prism testing period (leaching effect), with the exception

of the Po and Su aggregates (Figure 2.2B). The trend for levelling off of the expansion process is also visible for several aggregates in field test blocks, with a few exceptions (Figure 2.2C). Figure 2.2D compares the 14-day (AMBT) and 52-week (CPT) expansions plotted against the 20-year field test block expansion (15 years for Vir and Wt). Two anomalies (Vir and Po) are observed with the AMBT results, where grinding to sand-size particles for mortar bar testing "destroys" the texture of the reactive material, thus resulting in *false negative* results [19,20]. On the other hand, many studies reported *false positive* results associated with the AMBT. Medeiros et al. [21] for instance showed that several magmatic rocks of basic composition generate high AMBT but limited CPT expansions due to temperature activation of volcanic glass or zeolite material in the former. Users should be aware of potential anomalies resulting in misleading results under accelerated laboratory conditions, as neither the AMBT nor the CPT can accurately capture the "reactive/expansive character" of all rock types.

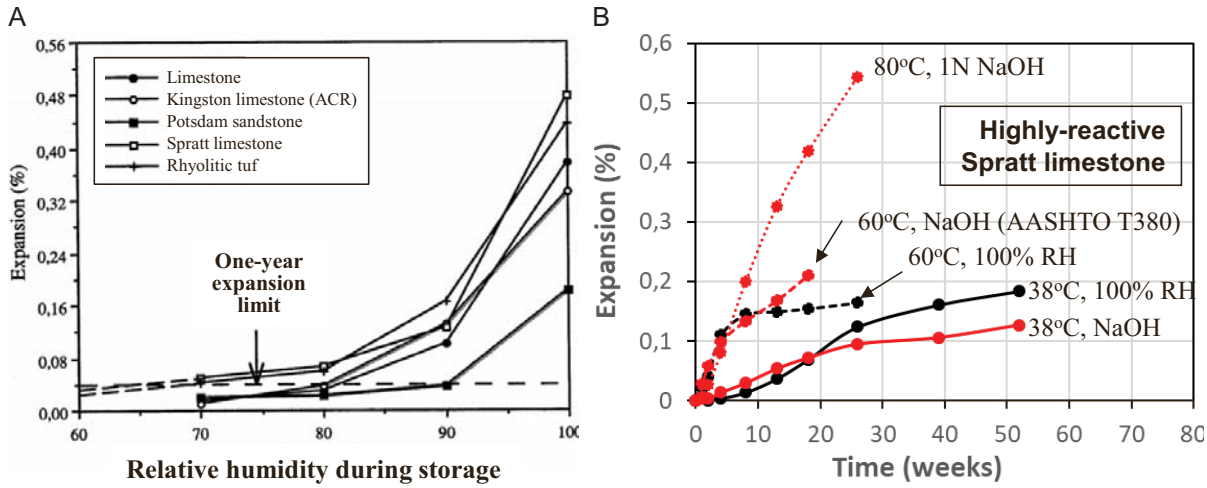

Figure 2.1: A. Expansion vs time of concrete prisms, 75×75×300 mm in size, made in accordance with CSA A23.2-14A, with different aggregates, and stored under different RH conditions (38°C) [12]. B. Expansion under different storage conditions for concrete prisms, 75×75×300 mm in size, made in accordance with CSA A23.2-14A CPT (alkalis boosted to 1.25% Na_2Oeq) and with the Spratt limestone [22-24]; specimens in 1N NaOH at 60°C were tested according to AASHTO T380 Miniature Concrete Prism Test (MCPT) [25].

2.1.2 Effect of restraints on ASR expansion

The following sections describe the results of studies conducted to better understand the effect of restraints on concrete made with reactive aggregates. Most experiments were conducted in laboratory conditions, but one field case is also discussed.

Laboratory investigations

Le Roux et al. [26] subjected cores extracted from a bridge section showing map cracking to uniaxial stress (1, 3 or 5 MPa) in creep jigs immersed in water. Axial strains were monitored in both loaded and unloaded (free) specimens. The authors reported that an increase in the applied stress resulted in a steadily decreasing expansion. At a stress level of 5 MPa, the expansion was almost eliminated, while it reached 0.7% in free specimens.

Larive [27] studied the behavior of non-reactive (control) and reactive concretes under moist conditions (RH > 95%) and constant uniaxial stresses (5, 10 and 20 MPa). Axial and transverse strains were monitored for all specimens. Creep tests were performed on the non-reactive concrete to determine the ASR-imposed strains by superposition, assuming identical creep behavior in the reactive and non-reactive concrete specimens. At stresses of 5 and 10 MPa, a maximum axial ASR-imposed strain of 0.03% was obtained, while it was practically eliminated at 20 MPa. The transverse strains increased up to a uniaxial stress of 10 MPa and then decreased at 20 MPa; this was explained by the presence of microcracks of mechanical origin at a stress of 20 MPa (50% of the compressive strength) that could be filled by ASR gel without causing deleterious pressures. The author reported comparable ASR-imposed volumetric strains in free specimens and in those subjected to 5 and 10 MPa stress levels; however, the volumetric strains are reduced at a stress level of 20 MPa.

A B

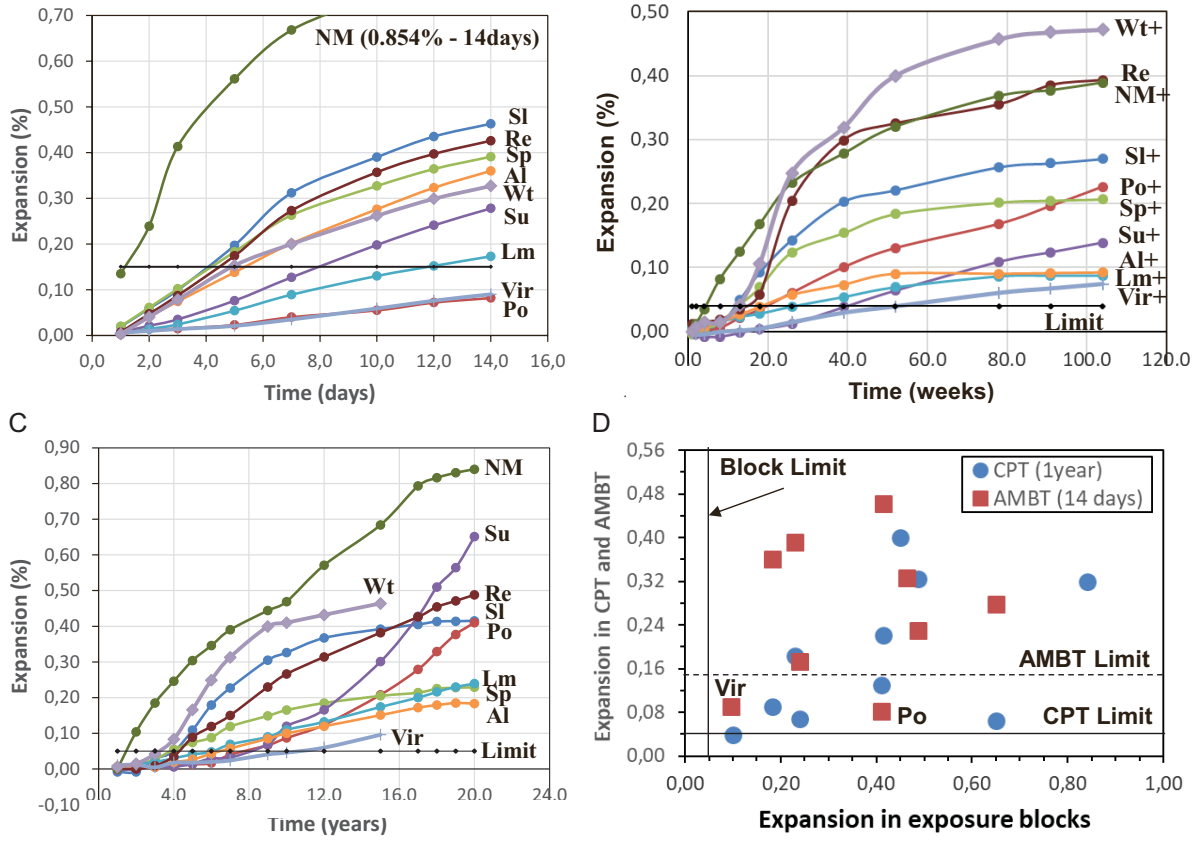

Figure 2.2: Expansion against time from various reactive aggregates in the AMBT (A), CPT (B) and field test blocks (CANMET exposure site) [18,23] (C). D. Plot of the 14-day (AMBT) and 52-week (CPT) expansions against field test expansion. Reactive coarse aggregates: NM - New Mexico polymictic gravel (USA); Su - Sudbury polymictic gravel (Canada); Re - Volcanic aggregate (Australia); Sl - Springhill greywacke (Canada); Po - Potsdam sandstone (Canada); Lm - argillaceous limestone (Canada); Sp - Spratt limestone (Canada); Al - polymictic gravel (Canada); Vir - granitic/gneiss (USA). Reactive fine aggregate: Wt - Wright (USA).

Multon and Toutlemonde [28] investigated the behavior of reactive concrete in sealed condition and uniaxial, biaxial, and triaxial confinement states. The experiments were carried out in creep jigs with axially applied stresses of 10 and 20 MPa. Creep tests were conducted on non-reactive concrete to determine the ASR-imposed strains by superposition. Some specimens were confined in steel rings (3 and 5 mm in thickness), thus resulting in triaxial (specimens loaded in the frames) or biaxial (unloaded specimens) stress conditions. Due to the use of steel rings (passive restraint), the confining pressure increased with the advancement of the reaction. The concept of "expansion transfer" is illustrated in Figure 2.3A, where the anisotropy coefficient is shown as a function of the normal component of the stress deviator in the axial direction ($\sigma_{zz} - \sigma_{mean}$). Figure 2.3B shows the ASR imposed volumetric strain as a function of the average or volumetric stress. No relationship between the ASR imposed volumetric strain and the stress state can be clearly defined, thus suggesting that volumetric strain is conserved.

In the triaxial tests conducted by Multon and Toutlemonde [28], the confining pressures evolved with the advancement of the reaction. For triaxial testing with isostatic and constant stress states, Liaudat et al. [29] showed that the ASR-imposed volumetric strain rate decreases nonlinearly with increasing stress level. By extrapolation, the rate becomes zero at an isostatic stress of the order of 10 MPa, suggesting that the volumetric expansion can be mitigated under triaxial confinement conditions. Gautam et al. [30] reported a significant decrease in volumetric strain under triaxial conditions, while the volumetric strain in the uniaxial and biaxial conditions was similar to that occurring in the free condition (Figure 2.4).

Dunant and Scrivener [31] studied the behavior of reactive concrete under constant uniaxial stresses (5, 10, and 15 MPa) in experiments where the specimens were immersed in an alkaline solution. Axial and transverse strains were monitored on unloaded (control) and loaded specimens. Testing was performed on non-reactive specimens to determine the ASR-imposed strains by superposition. The expansion due to ASR was almost totally mitigated in the loading axis at 5 MPa (0.1 mm/m), while it was zero for 10 and 15 MPa. The transverse strains were always lower for the axially loaded specimens

compared to the unloaded control specimens. Furthermore, the lowest transverse strain was observed for a stress of 5 MPa, and then increased for stresses of 10 and 15 MPa. Contrary to the previous studies [27,28,30], conservation of volumetric strain for a 1D stress state was not observed.

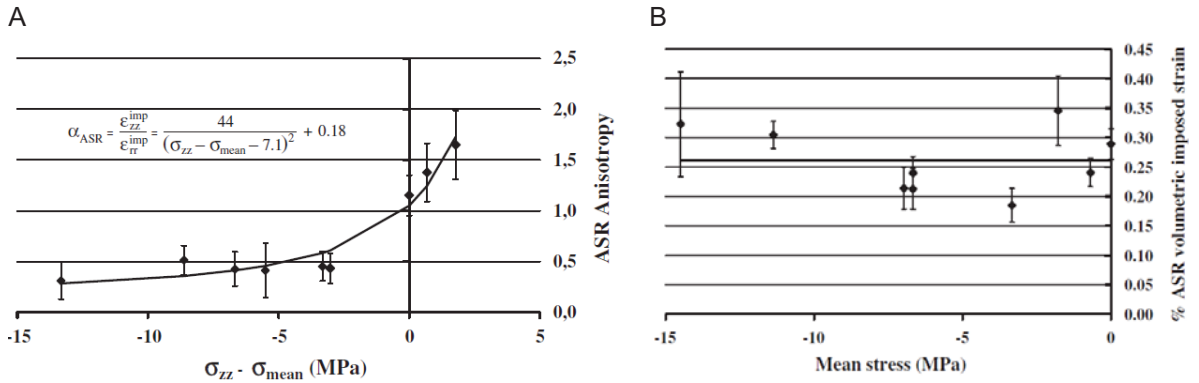

Figure 2.3: A. Expansion anisotropy as a function of the normal component of the stress deviator in the axial direction. B. Volumetric strain as a function of the mean stress [28].

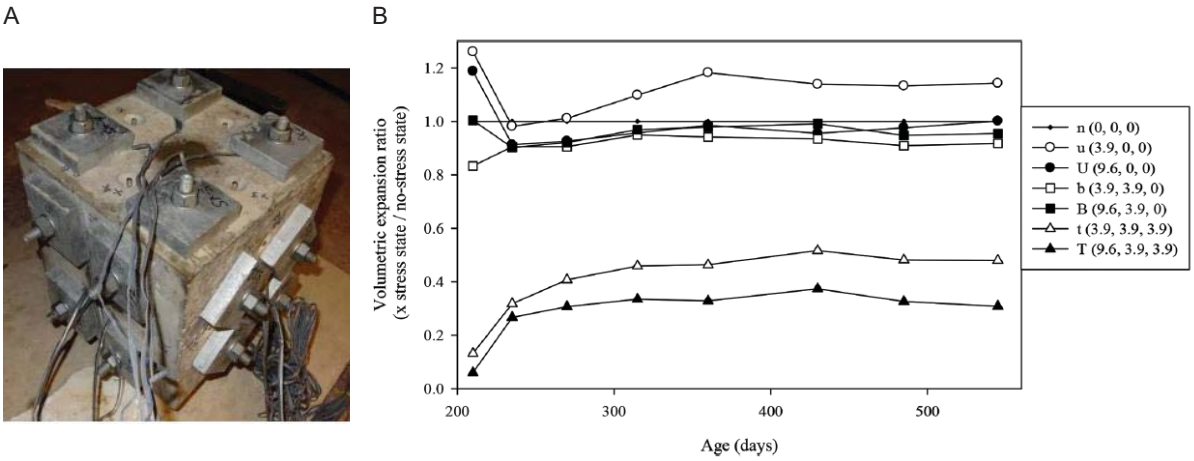

Figure 2.4: A. Triaxially loaded reactive concrete specimen. B. Evolution of volumetric strains in concrete for various stress states (null: $n(\sigma_x,\sigma_y,\sigma_z)$; uniaxial: $u(\sigma_x,\sigma_y,\sigma_z)$ or $U(\sigma_x,\sigma_y,\sigma_z)$; biaxial : $b(\sigma_x,\sigma_y,\sigma_z)$ or $B(\sigma_x,\sigma_y,\sigma_z)$; and triaxial: $t(\sigma_x,\sigma_y,\sigma_z)$ and $T(\sigma_x,\sigma_y,\sigma_z)$, where $\sigma_x,\sigma_y,\sigma_z$ (e.g. 3.9 and 9.6) are the applied stresses [MPa] in the x-, y-, and z- axis directions) [30].

The studies on the influence of stresses on ASR affected concrete have generally been carried out on so-called conventional concretes characterized by moderate aggregate sizes (25 mm and less) and w/cm ranges typical of structural applications. Yet, many massive structures such as dams and power plants are affected by ASR. Compared to concrete mixtures for structural applications, mass concrete mixtures have typically larger particle sizes, lower paste content, and higher w/cm. These specific mixture characteristics may exert a significant influence upon the expansive behavior due to ASR and the resulting damage under different stress states.

As part of a research program aiming at evaluating the effect of ASR on the mechanical properties of a mass concrete mixture identical to that used in a hydraulic dam showing important signs of ASR in the Northwestern part of the province of Quebec (Canada), Essalik et al. [32] studied the behaviour of cylindrical concrete specimens under the six different stress states illustrated in Figure 2.5A and 2.5B, either exposed to 100% R.H. or sealed, and both at 38°C (Figures 2.5C and 2.5D). The specimens consisted of cores, 150 × 300 mm in size, extracted from large laboratory-made concrete blocks (cement dosage of 240 kg/m^3, w/cm of 0.60 and coarse aggregate particles of 5 – 40 mm in size, concrete alkali content raised to 4.6 kg/m^3 with the addition of NaOH for expansion acceleration purposes). The specimens subjected to a non-zero axial stress (σ_x) were loaded in creep jigs, while lateral confinement (σ_y, σ_z) was ensured by means of metallic rings. The rings were installed with a clear distance (19 mm) in between them, in order to allow moisture exchange in the test series conducted at 100% RH (Figure

2.5C). Confinement rings with different thicknesses (6.35 mm, and 9.53 mm) were used, providing restraint levels similar to those reported in [28] (Figure 2.5C).

Figure 2.6 shows the longitudinal and transverse strains recorded for specimens under sustained axial stress of 10 MPa in the two investigated moisture conditions (100% RH and sealed). The results indicate that an external water supply is necessary for the reaction to develop, as little reaction/expansion developed in sealed specimens. A lateral expansion of 0.182% is reached at 333 days in moist condition (2.6A), while it is only 0.019% at 378 days in the sealed condition (2.6B). In Figure 2.6A, one can see that lateral expansion for the specimens confined with rings is much lower due to the passive restraint provided. In the axial direction for the moist and sealed conditions, an initial elastic strain due to the application of the load is first observed. The recorded contraction keeps increasing over time due to creep and the strains recorded in the moist and sealed conditions are observed to be close for a period of about 50 days. The corresponding curves then begin to diverge, almost stabilizing for the specimens in moist condition (2.6A) whereas they continue to decrease for those in sealed condition (2.6B). This difference can be explained by a much higher reaction rate in moist condition. With the assumptions that ASR in sealed condition is negligible, and that creep between moist and sealed specimens is similar, it is estimated that the axial ASR imposed strain in moist specimens at 378 days is on the order of 0.1%.

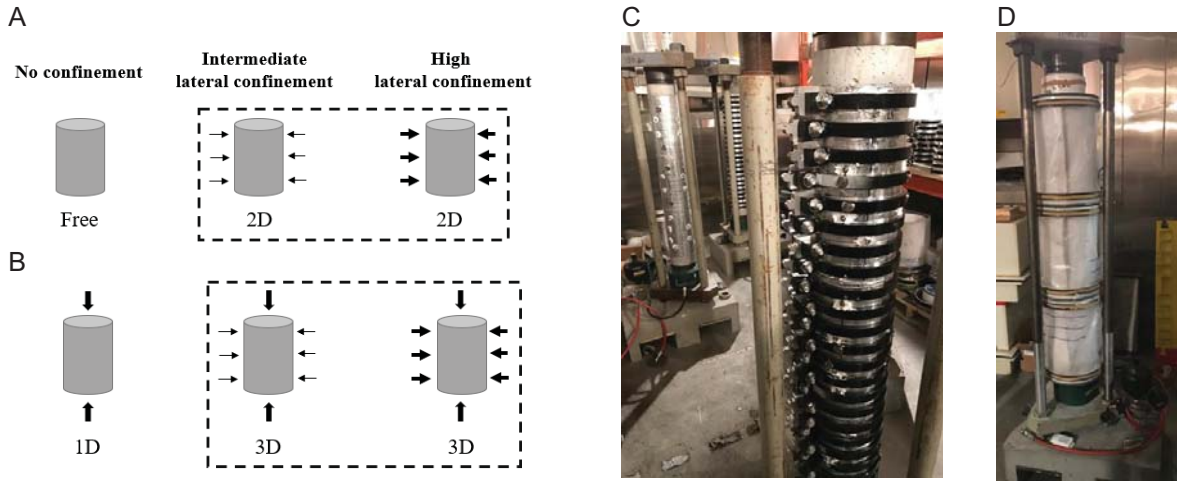

Figure 2.5: Stress states imposed to concrete specimens in the different test series: A. No axial stress applied, but different levels of lateral confinement; B. Specimens subjected to an axial stress and different levels of lateral confinement. Experimental setups: C. Sealed specimens loaded axially, respectively without confinement rings (back left) and with confinement rings (front right); D. Specimens exposed to 100% RH and loaded axially (confinement rings inside the moisture jacket) [32].

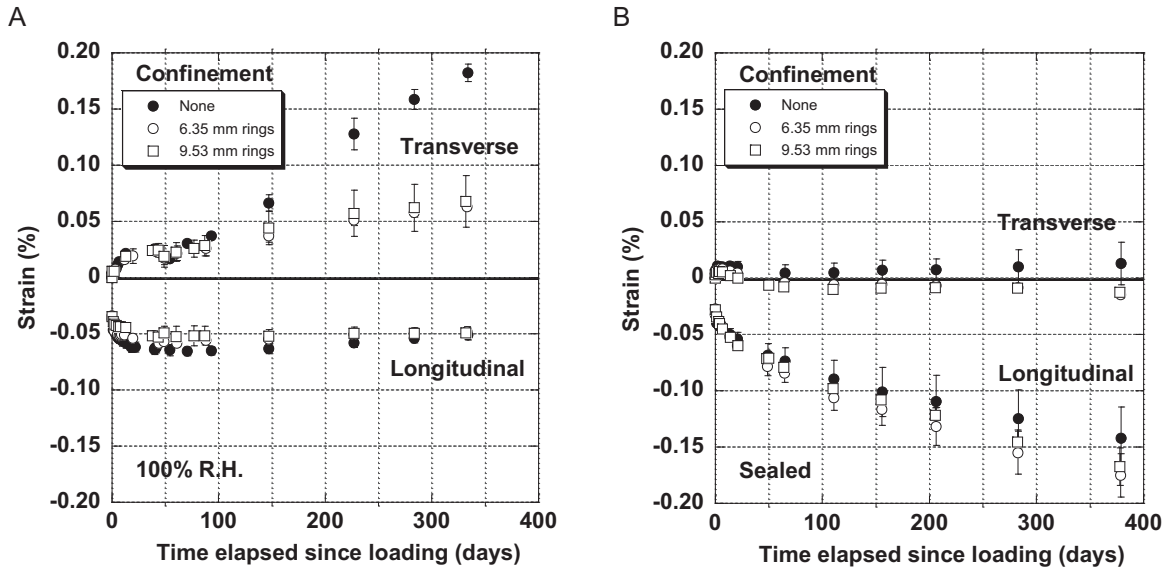

Figure 2.6: Longitudinal and transverse strains for concrete cylindrical specimens under a sustained axial stress of 10 MPa and different levels of lateral confinement (no confinement; 6.35 mm thick rings; 9.53 mm thick rings). Moisture condition: A. 100% RH; B. sealed specimens. [32].

In order to simulate the behaviour of ASR-affected thick concrete slabs without shear reinforcement, as observed in the Robert Bourassa-Charest overpass (Quebec City, Canada) (Figure 2.16A), two sets of four reinforced concrete slabs, 610×750×4500 mm in size, were manufactured using a concrete mixture prepared with a high-alkali (HA) cement and highly reactive gravel aggregate from New Mexico [33-35]. The slabs incorporated a bottom layer of ten 25M (cross-sectional area of 500 mm^2) steel rebars (1.18% of reinforcement in flexure) bent at the end of the specimens (Figures 2.7A and 2.7B), three 10 M rebars (cross-sectional area of 100 mm^2) in their upper part (shrinkage control), and three 10 M rebars (stirrups) installed near each end [35]. Stainless steel gage studs (38 mm-long) were installed on three surfaces of each slab to monitor their longitudinal, vertical and transversal deformations during storage at 38°C and >95% RH. The rebars at the bottom of the slab confined the concrete both in the longitudinal and the transverse directions; the confining effect diminished towards the top of the slab and, incidentally, the longitudinal expansions measured at a given level on the side of the slabs increased with the distance counted from the bottom steel reinforcement [34,35] (Figure 2.7C and 2.7D). As a result of the differential restraining conditions between the bottom and top of the test slabs, the expansion due to ASR induced a distortion of the initially rectangular cross-section, which became somehow trapezoidal.

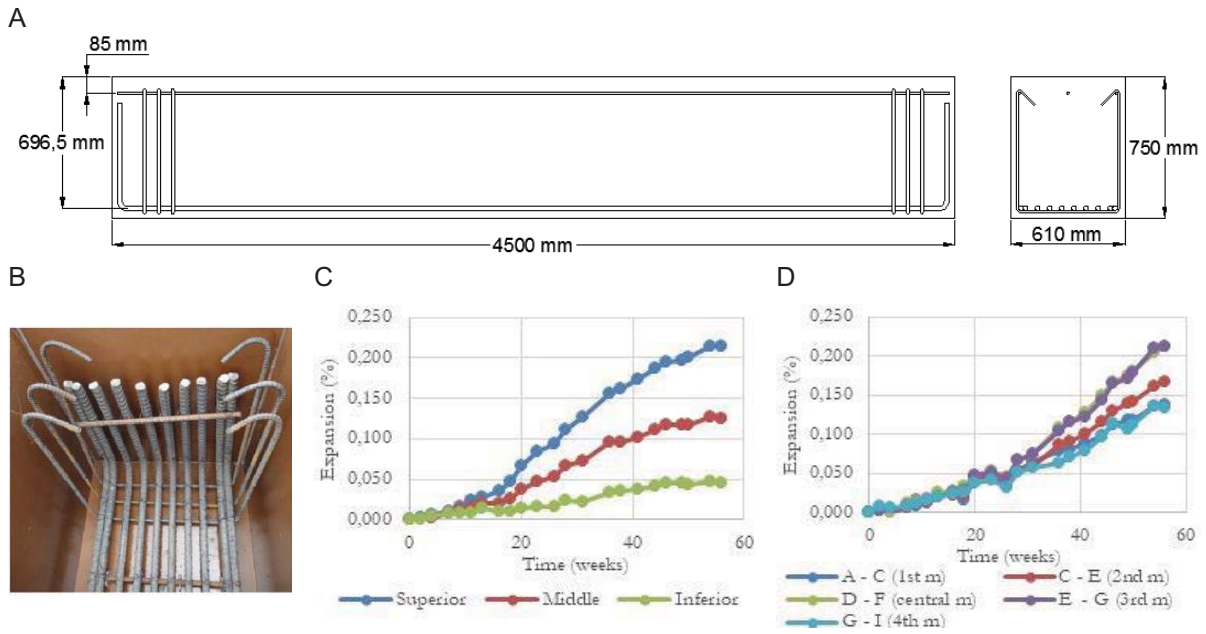

Figure 2.7: A & B. Design/details of the thick-slab sections. C. Average longitudinal expansion on the side face of slab 2-R3. D. Average vertical expansion on the side face of slab 2-R3 [33-35]; measurement sections A-C and G-I (lower expansion values) were located close to vertical bars at the ends of the slab, while sections D-F and E-G (higher expansion) were located in the middle portion of the slabs (away from vertical bars) [34].

Field case

The expansion under field conditions of reinforced and unreinforced concrete beams, 600×600×2000 mm in size (Figures 2.8A and 2.8B), made using concrete mixtures prepared with either high- (HA) and low-alkali (LA) portland cements (cement content of 415 kg/m^3) and the reactive Spratt limestone, is illustrated in Figure 2.8C. Gage studs consisting of 100 mm-long stainless-steel bolts were installed vertically in the upper surface of the concrete beams for longitudinal deformation monitoring. Sustained expansion is observed in the unreinforced HA- and LA-based concrete beams, but a trend for leveling off after about 20 years is observed [36,37] (Figure 2.8C). Both reinforced LA- and HA-based concrete beams stopped expanding after about 12 years and showed identical expansion curves afterwards. Hooton et al. [37] reported that the presence of longitudinal steel reinforcement at a ratio of 1.41% restrained the expansion by approximately 40% relative to that of nonreinforced HA beams over a monitoring period of 20 years (Figure 2.8C).

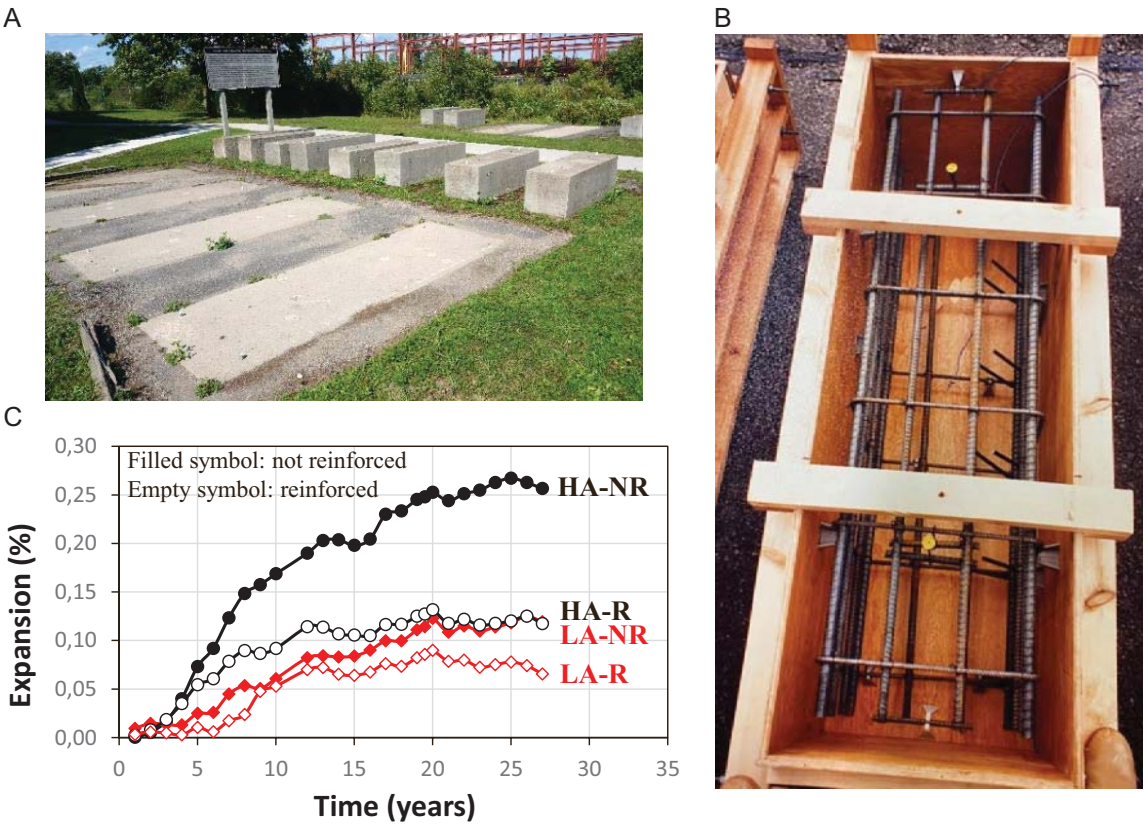

Figure 2.8: A. Test slabs/blocks cast in 1991 and stored on MTO's outdoor exposure site in Kingston (Canada). B. Reinforcement detailing in the reinforced concrete blocks. C. Expansion of reinforced (R) and unreinforced (NR) field test blocks made with concrete mixtures prepared with either low-alkali (LA) and high-alkali (HA) cements and incorporating Spratt limestone [36,37].

2.2 Cracking in concrete due to ASR

2.2.1 Generation of cracking/damage within ASR-affected concrete specimens

Effects of ASR gel composition and properties at the nano/microscale

Symptoms of damage within ASR-affected concrete specimens have been analyzed and described from the nano to the macro-scales in numerous studies. Amongst those, *cracking* is certainly the most widely reported. Barbotin-Albinski et al. [38] reported the results of Transmission Electron Microscopy (TEM) observations (nanoscale) on thin lamellae prepared from concrete prisms at early expansion levels (< 0.02%). "Early-stage products" of granular (amorphous) and platy (nanocrystalline) texture were identified within very fine (pre-existing) cracks in coarse aggregate particles; their composition varied in Si, K+Na contents along those cracks and Ca was confirmed to quickly incorporate those products.

Leemann et al. [39] reviewed the textural/compositional characteristics of secondary ASR products by Scanning Electron Microscopy and energy-dispersive X-ray spectroscopy (SEM + EDS). Crystalline (platy-like) ASR products are mainly found along cracks within reactive aggregate particles, while amorphous (gel-type) secondary products can be found towards the edge of those "aggregate" cracks (i.e. close to the ITZ), within cracks and air voids in the cement paste. The authors mentioned that the swelling capacity of the above products varies according to their location (inside the aggregate particles / cement paste), nature (amorphous / crystalline-platy) and composition (e.g. Na+K/Si, Ca/Si).

Using a thermodynamic approach, Larive [27] showed that the progression of the chemical reaction and mechanical stresses may theoretically be coupled; however, scanning electron microscopy (SEM) analysis revealed that the rate of gel production was similar in loaded and unloaded specimens, suggesting no effect of the stress levels investigated (5, 10 and 20 MPa) on the rate of gel production.

Urhan [40] summarized the results of several studies and suggested that the transition from a low viscosity alkali-silica gel to C-S-H is followed by a change in the gel's physical and mechanical properties

(Figure 2.9). High-calcium gel is more rigid and show limited swelling capacity, whereas low-calcium gel has a high swelling capacity and a lower viscosity [40].

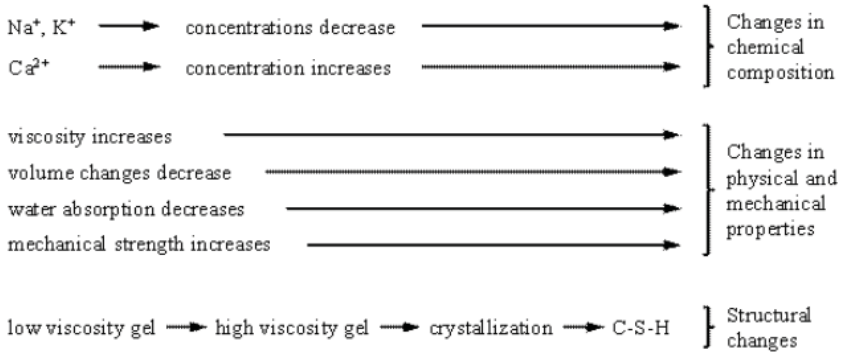

Figure 2.9: Changes in the nature and properties of the alkali-silica reaction product [40].

The ASR gel is a viscoelastic substance [41,42]. The confinement provided by the surrounding environment and the application of external stresses could allow the gel to creep and thus significantly reduce the swelling pressure. Furthermore, according to Gholizadeh-Vayghan et al. [42], the viscoelastic properties of the ASR gel affect its rheology and thus its restrained swelling pressure and the resulting damage/cracking to concrete. They showed that gel properties are highly dependent on chemical composition, specifically the molar ratio of Ca/Si, Na/Si and K/Si. An increase in the gels' alkali content (Na+K)/Si led to drastic decrease in the stiffness and viscosity of the gels. Meanwhile, increasing the Ca/Si ratio generally increased the gels' stiffness and viscosity in a nonlinear manner.

Signs of ASR at the macro (mm) scale

Cement paste and aggregates composing concrete are said to be quasi-brittle materials where energy is dissipated by cracking in the principal directions once the tensile strength is reached. Swelling of the ASR gel creates deleterious pressures that generate local tensile stresses and subsequent cracking. In a free state where the behavior is assumed to be isotropic, deleterious pressures will cause tensile stresses that will not be influenced by the orientation and the resulting cracking will be random (Figure 2.10A). The action of external loads and restraints to free deformations induce internal stresses that superimpose with the local stresses caused by the swelling of the ASR gel. Figure 2.10B schematizes the influence of a stress field on the local stresses caused by gel swelling. For instance, when external compressive loading is applied in one direction, stresses are superposed and the resulting tensile stresses in the loading direction decrease (Figure 2.10B). If the magnitude of the load is such that the tensile stresses are significantly reduced or even completely offset, the consequence is that cracking will be preferentially oriented in the loading direction.

A

B

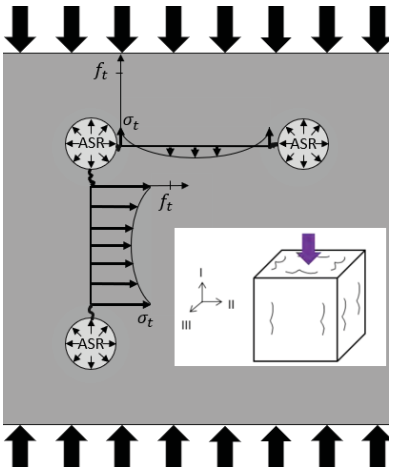

Figure 2.10: A. Map-cracking affecting field test blocks undergoing "free" expansion (CANMET exposure site, Ottawa, Canada). B. Evolution of the internal stresses and development of "oriented" cracking due to ASR under an uniaxial compressive stress (adapted from [43]).

When subjected to a sustained load, concrete not only undergoes an instantaneous elastic response, but continues to deform over time. This phenomenon is called creep [44]. The work of Troxell et al. [45] showed that total creep (basic and drying creep) of concrete specimens under controlled laboratory conditions (21°C and 50% R.H.) continues to increase after more than 20 years of testing. In structures affected by ASR, the reaction can similarly continue for decades, implying the potential of significant, long-lasting interaction between the ASR swelling pressures and creep of the cement paste. The development of stresses as a result of external loading or internally / externally restrained deformations cause some creep to occur simultaneously to the ASR activity. This interaction may contribute to the dissipation of swelling pressures and thus reduce the cracking propagation. The influence of creep would be more pronounced for particles showing a slower reaction [46]. Despite the difficulty in experimentally characterizing the influence of cement paste creep on deleterious pressures and damage, the mesoscopic model of Giorla et al. [46] indicates a significant influence.

The mineralogical nature of the aggregates and the type of reactive (siliceous) phase affect the reaction kinetics, the expansion process and the resulting macroscopic features of ASR that can be observed under stereobinocular/petrographic microscopes. Bérard and Roux [47] described the reaction mechanisms in field concrete specimens incorporating reactive “silicate” aggregates that included: 1) peripherical reaction in non-porous granites and gneisses with gel formation in the interfacial transition zone (ITZ) and cracking along grain joints (Figure 2.11A), 2) dissolution of reactive (sedimentary) cement within siliceous sandstone resulting in the formation of gel pockets within the particle and cracking radiating into the cement paste, and progressive disaggregation of the particles (Figure 2.11B); 3) formation of secondary reaction products within cracks in reactive aggregate particles (“white veinlets”) that extend into the cement paste with increasing expansion. The latter is a typical feature in “reactive” siliceous limestones (Figure 2.11C), argillite/siltstone, greywacke, chert, schist, quartzite, mixed volcanic rocks (e.g. rhyolite, andesite, tuff) (e.g. Figures 2.11D and 2.11E) [47-49].

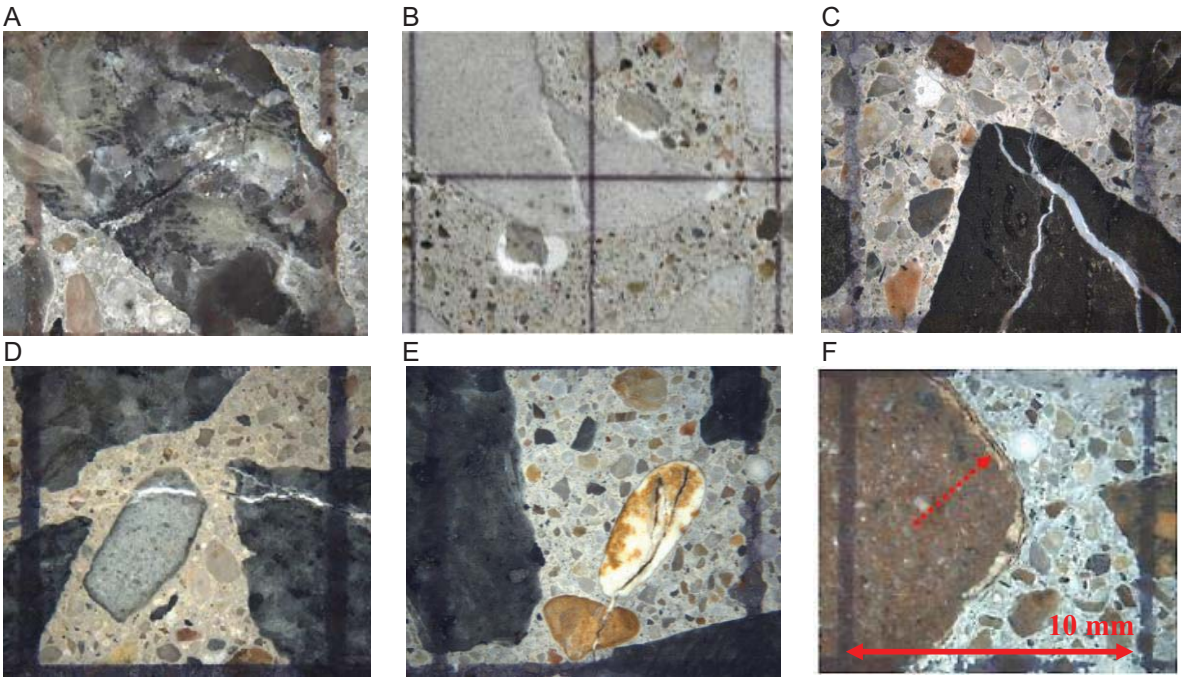

Figure 2.11: Macroscopic symptoms of ASR on polished concrete section (15× magnification). A. Internal cracking and grain joints within reactive granite/gneiss. B. Cracking and disaggregation of reactive siliceous sandstone with ASR product in air voids adjacent to the particle. C. White veinlet within a siliceous limestone particle and cracking extension into the cement paste. D. White veinlets within greywacke particles with connecting crack in the cement paste. E. Cracking partially filled with secondary reaction product and connecting crack between reactive chert fine aggregate particles. F. Peripherical cracking in the outer part of a volcanic aggregate particle [49].

Dunant and Scrivener [50] and Dunant and Bentz [51] described two different reaction types involving 1) rocks of homogeneous composition that react rapidly to generate cracking in their periphery and gel in the (surrounding) bulk cement paste at early stage of ASR, and 2) slowly reactive rock types creating gel pockets within the particles that induce internal cracking extending into the cement paste with progressing expansion. Reinhardt and Mielich [52] proposed somewhat similar ASR distress

mechanisms. The first involves dissolution at the surface of some reactive aggregate particles, with ASR gel and cracks forming at the ITZ and reaching the cement paste due to swelling pressures. The second involves the formation of gel pockets within aggregate particles whose swelling pressure induces cracks reaching the cement paste when the critical “crack length” is reached. Aggregate's toughness plays a critical role for crack extension. Pre-existing cracks or defects accelerate diffusion of ionic species from the pore solution into reactive aggregate particles to form swelling reaction products; the aggregate particle will crack once the critical stress intensity factor is reached [53].

Based on the petrographic examination of polished slabs prepared from 25, 35 and 45 MPa concretes incorporating a variety of reactive rock types, Sanchez et al. [53] proposed a “macroscopic” model (i.e. 10-15× under stereobinocular microscope) for ASR damage at different expansion levels (Figure 2.12A). *Sharp* (Type A – Figures 2.11A to 2.11E) and *onion skin* (Type B – Figure 2.11F) cracks can be identified within reactive particles. *Onion skin* cracks typically develop in rapidly reactive rock particles, similar to the first reaction described by Dunant and Scrivener [50] and Dunant and Bentz [51]. Cracks are mainly limited to reactive particles at low expansion levels, but then extend within the particles and into the cement paste with increasing ASR expansion. While new cracks form within the particles, it is easier for the expanding system to extend existing cracks than creating new ones. At high expansion levels (0.20/0.30%), cracks form a network connecting aggregate particles through their internal cracks or at the ITZ (Figure 2.12B).

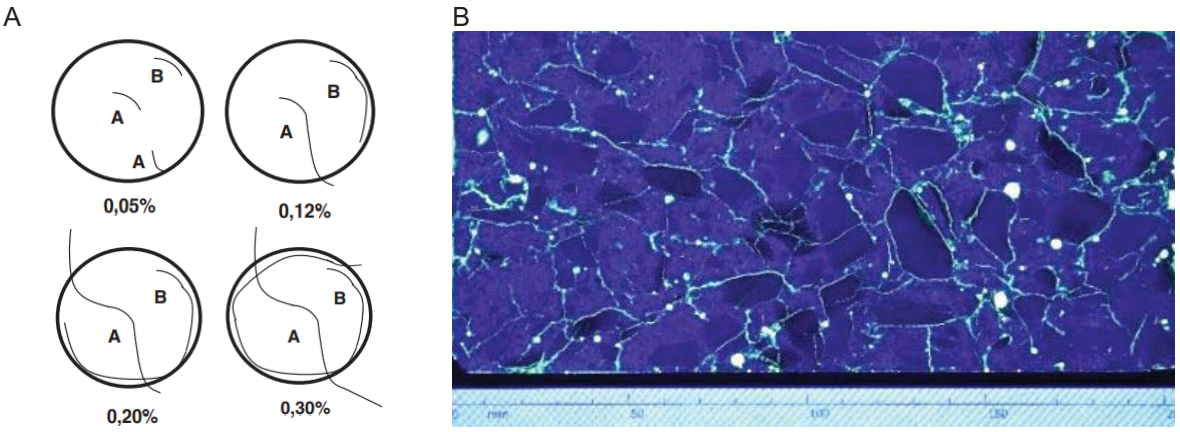

Figure 2.12: A. Qualitative model for the development of internal damage within ASR aggregate particles as a function of concrete prism expansion [53]. B. Polished concrete section impregnated with epoxy incorporating a UV tracer and showing cracking network between reactive aggregate particles (UV illumination; 35 MPa concrete, reactive limestone; 0.20% expansion) [54].

2.2.2 Quantifying/correlating expansion and internal cracking/damage within ASR-affected (unrestrained) laboratory concrete specimens

The deleterious process inducing concrete prism expansion can and actually must be confirmed through petrographic examination of test specimens. Sanchez et al. [53] found a strong linear correlation between the expansion of laboratory concrete specimens and their internal damage assessed by the DRI method. Similar rates of damage generation, mostly resulting from cracking development within aggregate particles and the cement paste, were observed for the wide range of reactive aggregates and concrete mix designs investigated, thus resulting in a tight envelope of DRI values when plotted as a function of the expansion results (Figure 2.13A); this suggests similar damage development in the concrete mixtures incorporating the different reactive rock types investigated. Lindgård et al. [55] also reported a good linear correlation between *Cracking Intensity*, measured as the relative surface area occupied by cracks in epoxy-impregnated polished sections (Figure 2.13B), and expansion for 15 test prisms incorporating a reactive Norwegian aggregate and representing a wide range of concrete types, laboratory exposure conditions and expansion levels (COIN project – [56]). Champagne [7] and Roy-Tremblay [8] assessed the damage and cracking levels in plane polished sections prepared from concrete prisms, also from the COIN project and representing 20 different combinations of storage conditions, concrete types and (four) reactive aggregates. The authors obtained similarly good correlations between the damage levels determined through either the DRI or Cracking Intensity (%) methods and the expansion results (Figure 2.13C and 2.13D).

Various studies confirmed the bias induced by alkali leaching on ASR expansion [14], which is illustrated in Figure 2.14A by the significant reduction in *Cracking Intensity* in the upper and lower portions of a concrete test specimen exposed to high humidity conditions in laboratory testing. RILEM AAR-13 method [57] proposes to wrap test prisms in alkali-impregnated cloths to mitigate this effect (Figure 2.14C). Using a petrographic procedure derived from the DRI method and consisting in evaluating damage within a set of longitudinal sections from the external to the inner part of concrete alkali-wrapped specimens (Figure 2.14B), Champagne [58,59] found higher damage in the outer portions (Line 1) of the specimen due to alkali ingress from the wrapping (Figure 2.14D). Actually, the analyzed concrete was made with the Spratt limestone (Canada), a low concrete alkali content of 1.5 kg/m^3, and the specimen was stored for 120 weeks at 38°C and 100% RH, a period over which it reached an expansion of 0.234%. With such a low original alkali content, not only did the alkali-wrapping of the test prism help mitigating the effect of leaching, but it likely boosted the expansion development in the specimen.

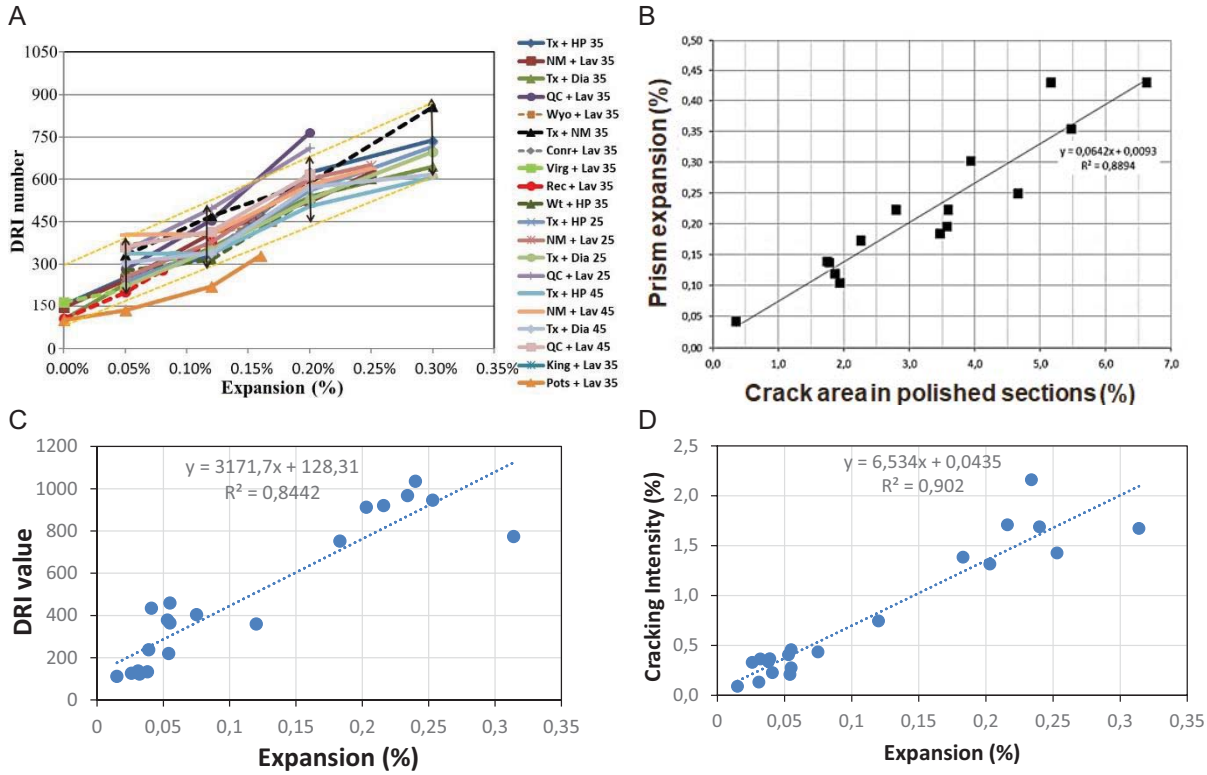

Figure 2.13: Correlation between the expansion and the internal damage of concrete specimens stored under laboratory conditions. A. DRI values against concrete prism expansion (38°C, 100% RH) for 25, 35 and 45 MPa concretes incorporating fine and coarse reactive aggregates [53]. B. Correlation between the crack area (%) determined by Image Analysis of impregnated polished sections and the expansion of concrete specimens [55]. C. DRI values against expansion for a set of 20 concrete prisms tested in the laboratory (38 and 60°C, different alkali contents, four rock types, control and SCM concretes). D. Cracking Intensity (%) determined by image analysis (same as in [55]) plotted against the expansion of the test prisms; same group of specimens as Figure C [7,8,56].

2.2.3 Surface cracking on ASR-affected structural concrete members

The visible pattern of cracking due to ASR on affected concrete structures is influenced by several factors, including mixture design characteristics, environmental conditions, as well as all variables that affect the stress fields such as the shape or geometry of the concrete element, reinforcement detailing, post-tensioning, other form of internal or external restraints, and the actual loading conditions. *Map-cracking* is a symptom of ASR (or other internal swelling mechanisms) occurring as randomly oriented cracks on the surface of concrete elements relatively free from restraints (Figures 2.16H). Conversely, surface cracking is typically observed to be oriented along the rebars and prestressing tendons.

Although compressive stresses can significantly reduce the expansion due to ASR in the direction of the stress field and cause the cracks to be oriented preferentially, in general, the extent of surface cracking is not significantly reduced by the use of internal or external strengthening [1]. For instance, more extensive cracking is observed on the surface of the high-alkali (HA) series beams (Figures 2.15D, 2.15E and 2.15F) compared to the low-alkali (LA) series beams (Figures 2.15A, 2.15B and 2.15C) on

MTO's exposure site, which correlates well with their higher expansion level (Figure 2.8C). However, significant surface cracking is still observed on both HA- and LA-based reinforced concrete beams, despite strong reductions in the measured expansions (Figures 2.8C, 2.15B, 2.15C, 2.15E, 2.15F).

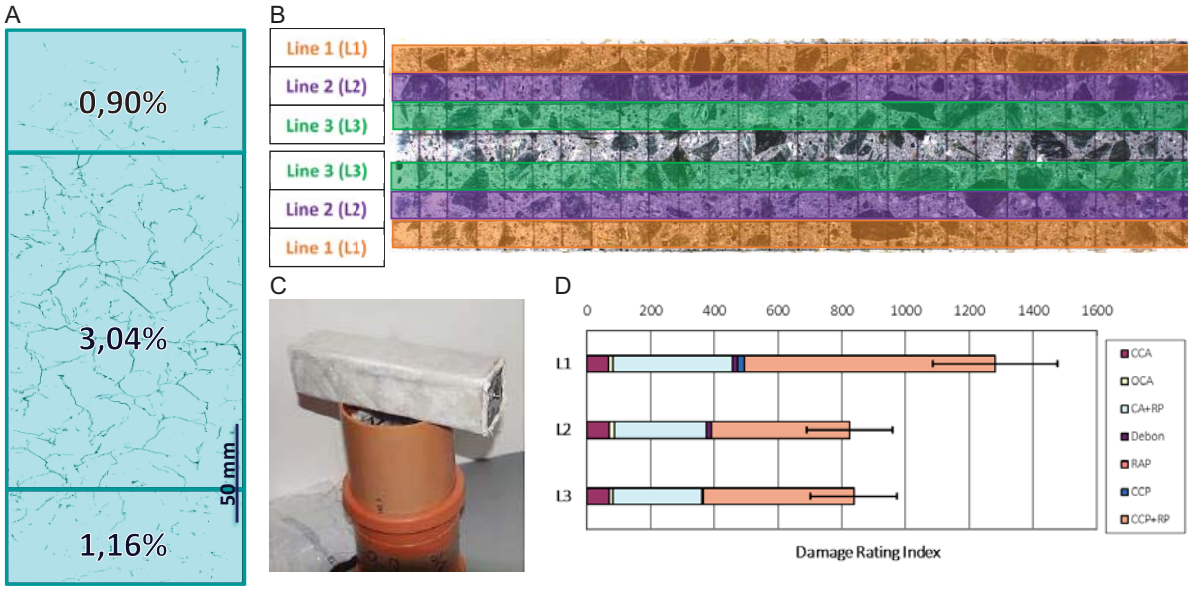

Figure 2.14: Effect of alkali leaching and wrapping on ASR expansion. A. Crack mapping highlighting leaching profile in a test prism subjected to laboratory testing (38°C, 100% RH). B. Polished section separated in three groups of two *lines* located at equal distance from the prism side surface (*Grouped lines approach for damage profiling*). C. Alkali-wrapping set-up for specimens used in the COIN project [56]. D. Distribution of damage (acronyms defined in Figure 2.17) from the external layer (L1) to the core (L2 and L3) of an alkali-wrapped concrete specimen [7].

In ASR-affected reinforced concrete members, expansion develops mainly in the direction of least confinement and cracking parallel to confining stresses. In ASR-affected columns of the Robert Bourassa-Charest overpass, for example, cracking developed preferentially along the longitudinal axis due to the confinement provided by the main reinforcement (Figure 2.16F). A similar effect can be seen in other types of concrete elements subject to very high ASR-induced stresses. An ASR-affected concrete pavement located in Bécancour (Canada), built in the 1960's but never opened to traffic, exhibit extensive map cracking on most pavement sections, away from the joints (Figure 2.17A). Next to these, where the slab ends came into contact and led in a number of cases to bursting, the state of stress caused cracking to develop longitudinally (Figure 2.17B). In a hydraulic dam affected by ASR, expansion generally occurs more freely in the upstream direction, resulting in predominant horizontal cracking in the downstream part [60], as can be seen in the example of Figure 2.18.

The availability/supply of external moisture is of paramount importance for the development of expansion and cracking due to ASR. Inner concrete columns of the Robert Bourassa-Charest overpass, mostly protected from the rain and solar radiations, showed significantly less surface cracking compared to side columns (Figures 2.16F vs 2.16G). Similarly, slab sections of the ASR-affected pavement in Bécancour that are located under a bridge structure crossing over the pavement (Figures 2.17C & 2.17D) showed limited surface cracking compared to that observed on the exposed portions of the pavement (Figures 2.17A and 2.17B) [61].

2.2.4 Correlating external (visible) and internal cracking/damage within ASR-affected concrete members

In general, the condition of a concrete structure is first assessed through visual surveys, notably from the extent of cracking affecting its various elements [62]. The question thus arises whether the severity of surface cracking is a good indication of internal damage and/or of the extent of expansion reached to date in the structural members examined. This is of critical importance for engineers interested in the management of aging concrete structures.

A – LA concrete beams; plain (#5) and reinforced (#5R) beams

D - HA concrete beams; plain (#6) and reinforced (#6R) beams

B – LA concrete beam, plain

C – LA concrete beam, reinforced

E – HA concrete beam, plain

F – HA concrete beam, reinforced

Figure 2.15: Plain (not reinforced) and reinforced field test beams, 600×600×2000 mm in size, incorporating the highly-reactive Spratt limestone and a low-alkali (LA) (A,B and C) and high-alkali (HA) (D, E and F) portland cements (Ontario Ministry of Transportation outdoor exposure site in Kingston, Canada). Condition (surface cracking) after 27 years of outdoor exposure. B: Plain concrete (P) beam made with the LA cement concrete mixture. C: Reinforced (R) concrete beam made with the LA cement concrete mixture. E: Plain (P) concrete beam made with the HA cement concrete. F: Reinforced (R) concrete beam made with the HA cement concrete mixture.

Figure 2.16: Robert Bourassa-Charest overpass (Quebec City, Canada). A. General view of the structure. B. Extraction of large concrete cores (about 800 mm in diameter) from the thick deck slab. C. Longitudinal reinforcement at the bottom of the thick deck slab. D. View of extensive cracking under the bridge deck and locations of two extracted (large) cores. E. Recovering of longitudinal, transverse and vertical specimens in the large core extracted from the bridge deck (B and C). F. Extensive longitudinal cracking in a section of a Y-shape exposed concrete column (see A). G. Limited cracking in a section of a Y-shape protected column. H. Map-cracking in the exposed portion of a foundation block supporting the Y-shape columns (see A).

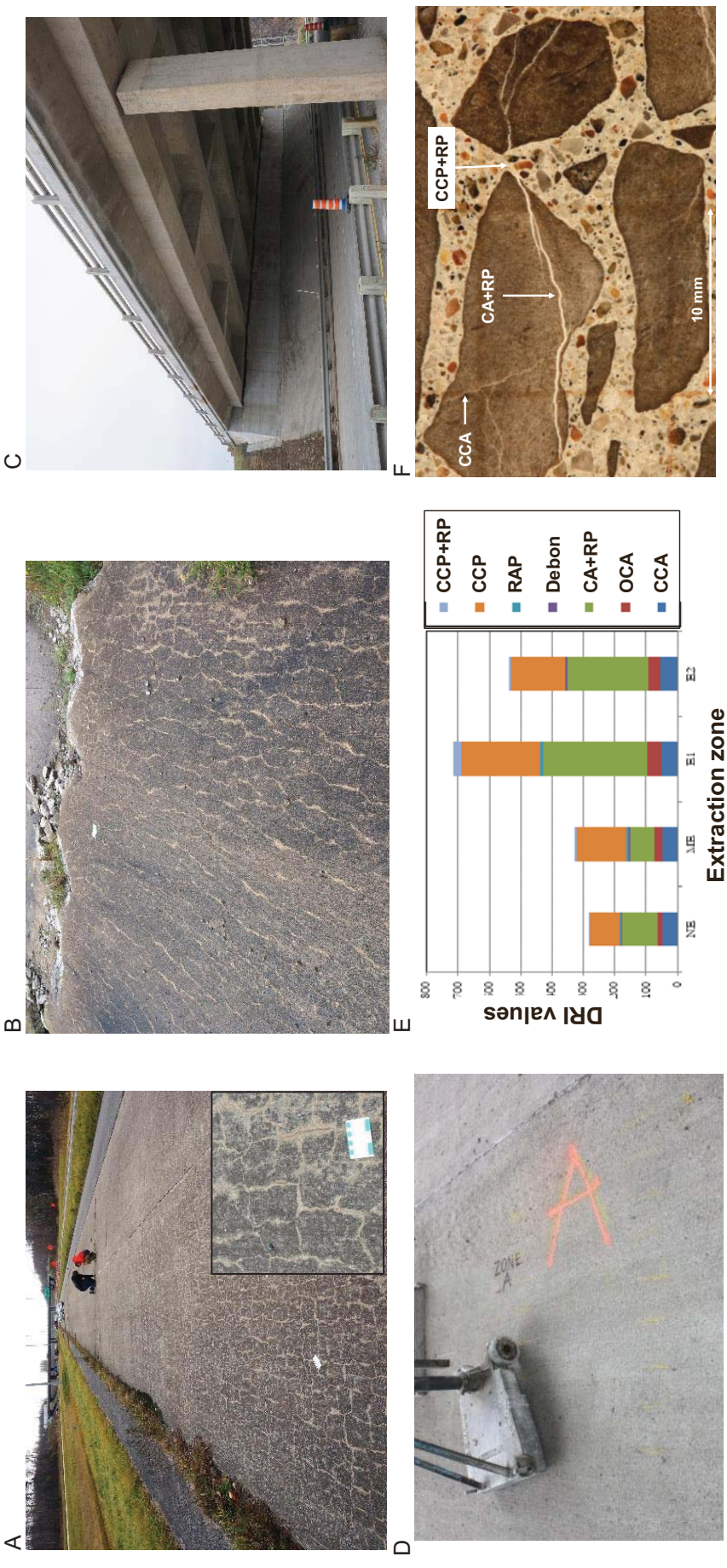

Figure 2.17: ASR-affected concrete pavement in the Bécancour area (Canada). A. General view of the pavement with extensive map cracking (section E1 in Figure E). B. Longitudinal cracking close to a burst joint. C. Bridge over the pavement section. D. Sheltered portion of the concrete pavement (under the bridge deck) showing limited surface cracking (section NE in Figure E). E. DRI results obtained from cores extracted from various pavement sections. NE: visually undamaged section (Figure D). ME: moderately-damage section. E1 and E2: Heavily damaged section (Figure A). [CCP+RP: cracks with reaction products in the cement paste; CCP: cracks in the cement paste; RAP: coarse aggregate corroded; Debon: coarse aggregate debonded; CA+RP: cracks with reaction products in the coarse aggregates; OCA: open cracks in the coarse aggregate; CCA: closed crack in the coarse aggregate]. F. Typical signs of ASR (cracking with secondary reaction products within the aggregate particles and the cement paste) in concrete pavement sections. [61].

Figure 2.18: ASR-affected concrete dam in Southern Quebec (Canada). A. General view of the dam with sawn surface for construction of new spillways and where coring locations are identified (red dots). B. Extensive horizontal cracking in the downstream face of the dam. C. Sketch from Figg [60] showing predominant horizontal cracking in the downstream part of an ASR-affected dam. D. DRI values from cores extracted in the mass concrete part of the dam (Fig. A) [CrCA: closed crack in the coarse aggregate; OCrCA: open cracks in the coarse aggregate; Cr+RPCA: cracks with reaction products in the coarse aggregates; CAD: coarse aggregate debonded; CrCP: cracks in the cement paste; Cr+RPCP: cracks with reaction products in the cement paste]. F. Typical symptoms of ASR (cracking with secondary reaction products within the aggregate particles and the cement paste) in the concrete.

Concrete members undergoing internal expansion due to ASR and experiencing cyclic wetting and drying typically show cracking of the skin layer, less expansive (alkali leaching/dilution processes, variable humidity conditions, etc.) and subject to the thrust exerted by the more expansive concrete core [63,64] (Figure 2.19). The *Cracking Index* (CI) method, which consists in measuring and summing crack widths over a reference grid drawn on the surface of a concrete element, can provide a quantitative assessment of the extent of cracking in structural members subjected to different exposure/restraint conditions. For example, in the case of a bridge structure in Norway, measurements along the circumference of heavily-cracked reinforced concrete columns showed higher CI values on the western columns (no.1) exposed to the dominating wind/rain direction and sun exposure (Figure 2.20) [59]. Periodic measurements of the CI allow to monitor the evolution of deterioration and may even be used to estimate the expansion reached to date by the affected concrete [3,9].

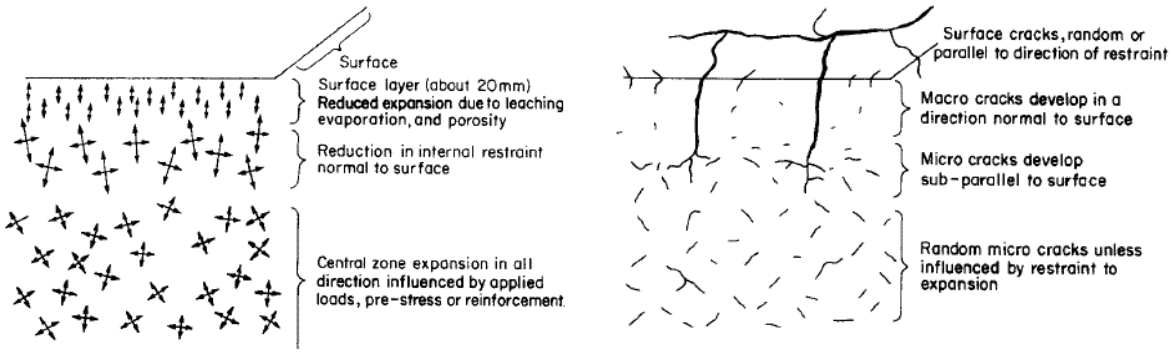

Figure 2.19: The surface layer of a concrete element exposed to outdoor conditions is likely to sustain alkali leaching and, as a consequence, to develop less expansion than the bulk concrete. This differential expansion between the surface and the core of the concrete element typically results in surface ("skin") macrocracking [64].

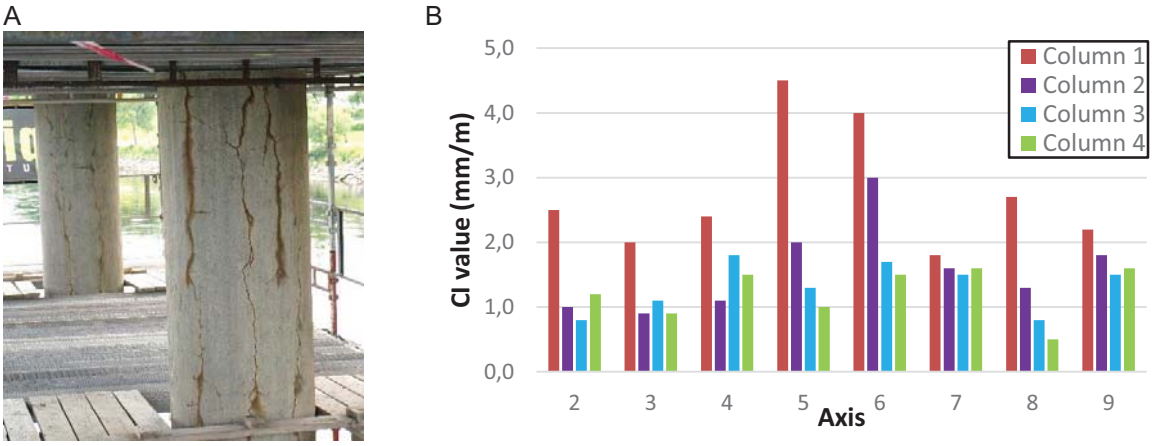

Figure 2.20: A. Extensive vertical cracking on concrete columns of a bridge in Norway. B. Cracking index (CI) values measured along horizontal lines drawn on the columns. In the graph, the title *Axis* corresponds to a given row of four columns in the transverse direction to the bridge orientation. In each row, Column 1 is located on the west side of the bridge [59].

In the early 1990's, field experiments were conducted on ASR-affected median barriers of the Robert Bourassa highway in Quebec City to evaluate the efficiency of silane/siloxane-based penetrating sealers in mitigating the progress of ASR deterioration [65]. Still today, untreated barriers show extensive ASR cracking in the exposed sections (Figure 2.21A), while those located under a bridge structure (protected from rain and solar radiations) and those treated with silane applications suffer from limited surface cracking (Figure 2.21B, 2.21C). In 2016, the total length of cracking in the upper part of the elements was assessed by image analysis (Figure 2.22A), while cores extracted from that zone (Figure 2.22B) were subjected to petrographic examination using the *DRI* method. The study indicated that 1) protection from moisture has a critical impact on the development of ASR cracking; 2) the silane-treated barriers, even after 25 years in service without reapplication, and the sheltered barriers developed significantly less signs of external/internal damage due to ASR (Figures 2.21D to 2.21F); and 3) a reasonably good linear correlation exists between the extent of surface cracking and internal damage in those thin structural elements (Figure 2.22C) [66].

The extent of visual surface cracking on the various sections of the pavement in Bécancour correlated well with the internal damage assessed through the DRI method (Figure 2.17) [61]. Limited cracking could actually be observed in the core from the sheltered pavement section (Figures 2.17C and 2.17D – NE in Figure 2.17E), as compared to the severe damage found in the exposed and heavily cracked sections (Figure 2.17A – E1 in Figure 2.17E) [61]. Extensive cracking with reaction products in the aggregate particles was observed, extending into the cement paste to form a network (Figure 2.17F). These features are identical to those observed in the barrier sections illustrated in Figure 2.21D, also incorporating a reactive siliceous limestone coarse aggregate.

Figure 2.21: Comparison of the external and internal cracking in barrier sections on the Robert Bourassa highway in Quebec City (Canada). Pictures A to C were taken after about 25 years in service. A. Untreated (control) section. B. Sheltered section (untreated) under bridge. C. Silane-treated (two applications) section. D. Signs of ASR in polished concrete core section from untreated barrier (DRI = 597). E. Signs of ASR in polished concrete core section from sheltered barrier (DRI = 122). F. Signs of ASR in polished concrete core section from silane-treated barrier (DRI = 237) [66]. The distance between vertical lines on D, E and F = 10 mm.

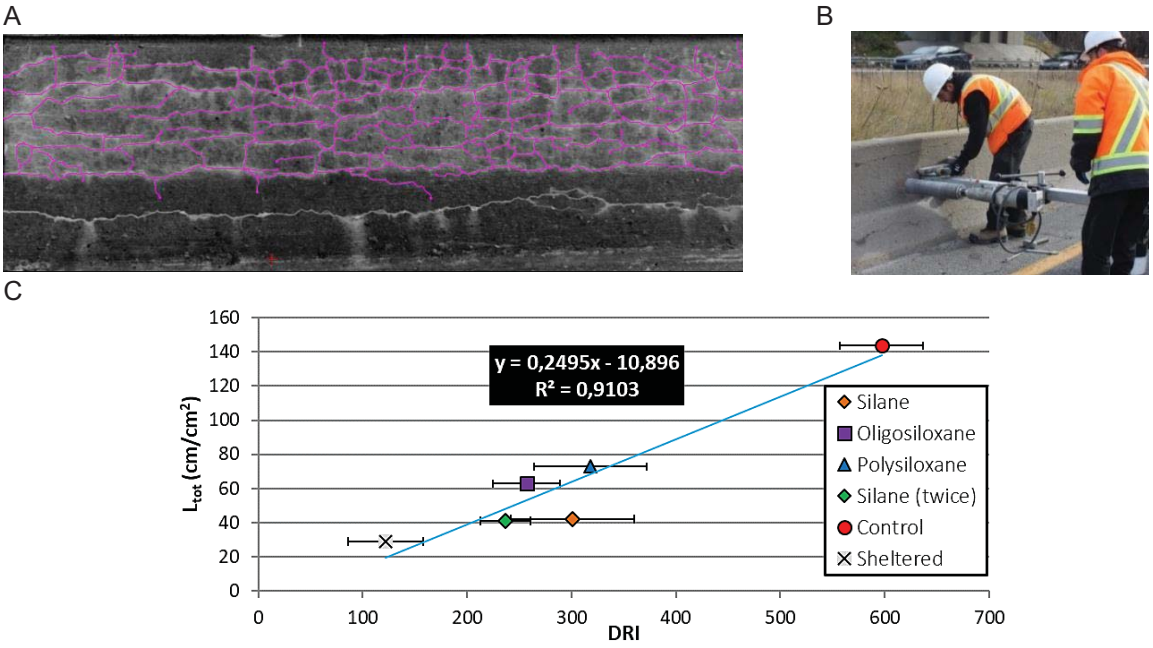

Figure 2.22: A. ASR-affected control (untreated) barrier section with surface cracking highlighted through Image Analysis. B. Coring location in the upper portion of the barriers. C. Correlation between surface cracking and internal damage (obtained by *DRI method*) in untreated/treated barrier sections [66].

2.3 Impact of ASR on the mechanical properties of concrete

Many studies conducted on specimens tested for free expansion in the laboratory showed that not all mechanical properties of concrete are equally affected by ASR. For instance, tensile strength (f_t) is considered a better indicator of ASR progression than compressive strength (f_c) [67-71], the latter being generally affected at higher expansion levels. For the various concretes tested, Sanchez et al. [72] found a reduction in f_t, measured through a gaz pressure method, reaching between 40 and 70% at 0.12% expansion, but levelling off rapidly afterwards (Figure 2.23A). They also found a progressive but limited reduction in f_c that reached a maximum of 35% at 0.30% expansion (Figure 2.23B). The modulus of elasticity (E_c) is strongly affected by ASR, even at early expansion levels [71-73]. Sanchez et al. [72] reported E_c reductions reaching between 25 to 50% and 45 to 70% at 0.12 and 0.30% expansion levels, respectively (Figure 2.23C). The rapid reductions of f_t and E_c are consistent with early-stage cracking development within the aggregate particles (Figure 2.23A and 2.23C). The *Stiffness Damage Index* (SDI) showed more progressive increase with increasing expansion, with a trend to level off above 0.20% (Figure 2.23D). This was attributed to the progressive filling of cracks with secondary reaction products that limits the energy consumed through the closure of cracks during testing. Similar trends could be observed for the various concretes tested, but the amplitudes varied according to the aggregate tested. Reinhart & Mielich [52] also highlighted the strong impact of the reactive aggregate types on the deterioration in the mechanical properties of ASR-affected concrete. Kubo & Nakata [74] and Giaccio et al. [75] attributed differences in the stress/strain behavior of ASR-affected concretes at similar expansions to variations in the characteristic cracking patterns of the different reactive aggregates.

Various experimental works have shown that the stress state can affect the damage measured at the macroscopic scale, through mechanical tests (strength, modulus of elasticity, SDT) [30,75-78], and at the microstructure scale, through the DRI test procedure [77,79]. The stress state affects the internal cracking pattern, which in turn affects the mechanical properties in all directions. Concrete that initially had isotropic behavior can then become anisotropic with the progress of the reaction. According to Gautam et al. [30] and Zahedi et al. [78], the change in elastic modulus showed a directional behavior with respect to the stress state and was observed to be anisotropic. Triaxial compressive stress in ASR concrete was observed to result in reduced volumetric expansion, lower DRI values, and less cracking [30]. Results reported by Zahedi et al. [78,79] demonstrate that ASR-induced expansion and deterioration change according to the direction and confinement configuration. Moreover, distinct crack features and orientations are generated in confined concrete (1D and 2D), which raises the question on whether ASR mechanisms are different under free and confined conditions.

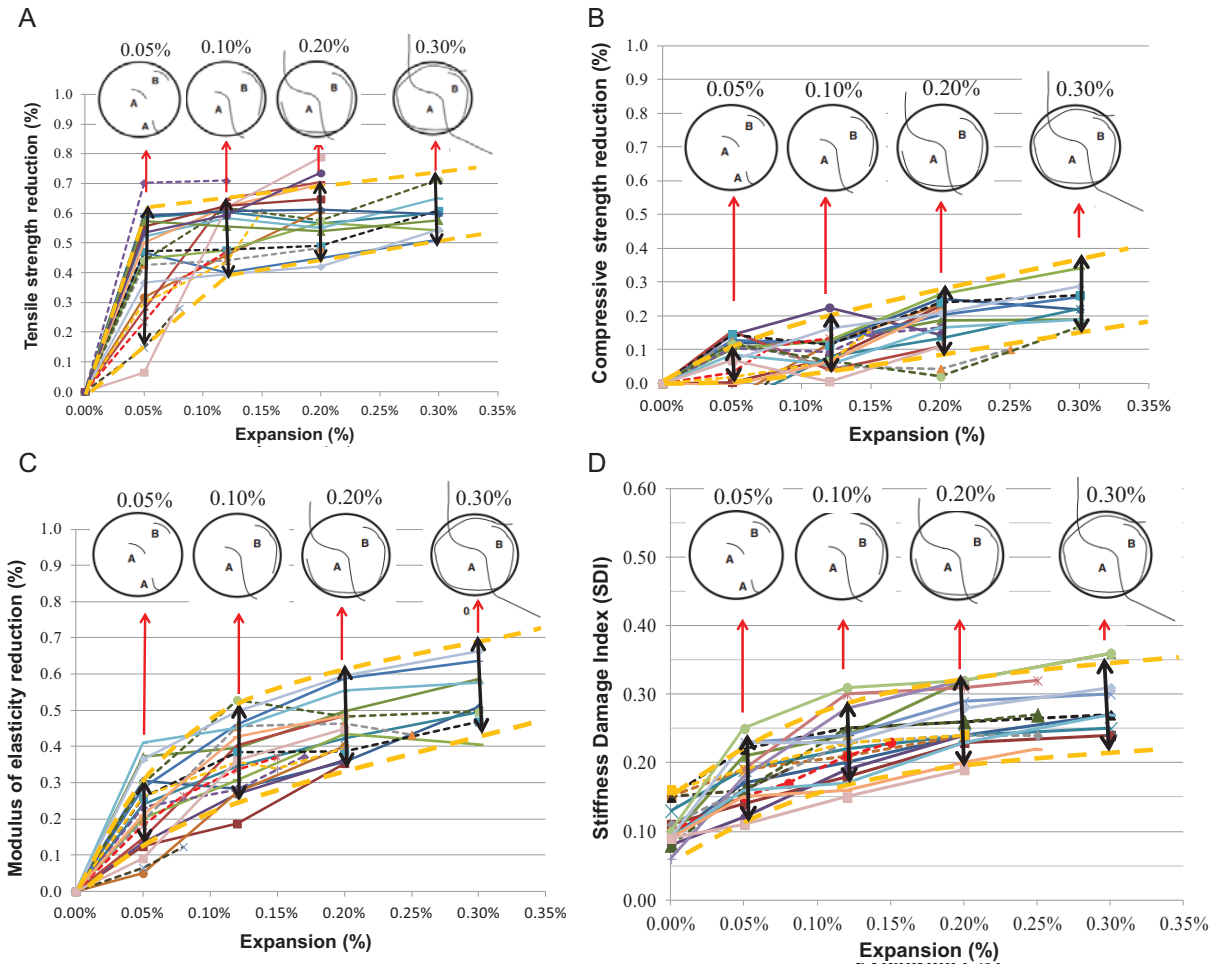

Figure 2.23: Evolution of ASR damage in concrete as a function of the (free) expansion of 25, 35 and 45 MPa concretes incorporating a variety of reactive coarse and fine aggregates [72]. A) Tensile strength reduction; B) Compressive strength reduction; C. Modulus of elasticity reduction; D. Increase in Stiffness Damage Index.

The effect of restraint on the mechanical properties and cracking development of concrete affected by ASR can be visualized in Figure 2.24 from the testing of core specimens extracted at different distances from the bottom reinforcement within the concrete slab sections described in section 2.1.2 and illustrated in Figure 2.7. Figure 2.24 presents on heat maps the loss in E_c, the SDI and the DRI values obtained on cores extracted from the moderately-damaged slab section 1-R2 (Figures A to C; reference expansion of 0.14%) and the highly-damaged slab section 2-R3 (Figures D to F; reference expansion of 0,23%) [35]. The results confirm that concrete damage due to ASR is increasing with the distance from the reinforcement [33-35], as the confinement effect gets less important.

Although the results of several studies suggested that compressive strength is likely not the best indicator of the extent of ASR in concrete, Barbosa et al. [76] showed that compressive strength is significantly affected by ASR cracking. The authors studied the mechanical properties of concrete cores extracted in the vertical and horizontal directions in sections extracted from bridge decks showing strong horizontal cracking (Figure 2.25). The strength in the direction perpendicular to ASR cracks (vertical drilling) was found to be significantly lower than that in the direction parallel to ASR cracks (horizontal drilling). Compressive strength reductions up to 64% and 52% were observed for vertically and horizontally drilled cores, respectively. The authors also indicated that Young's modulus is affected by crack orientation and that closure of cracks perpendicular to the loading axis resulted in up to 90% reduction in Young's modulus compared to that of the original, uncracked concrete. Care should thus be exercised in interpreting reductions in mechanical properties of concrete due to ASR, as it can be significantly influenced by the orientation of cracking present in the (drilled) core specimens.

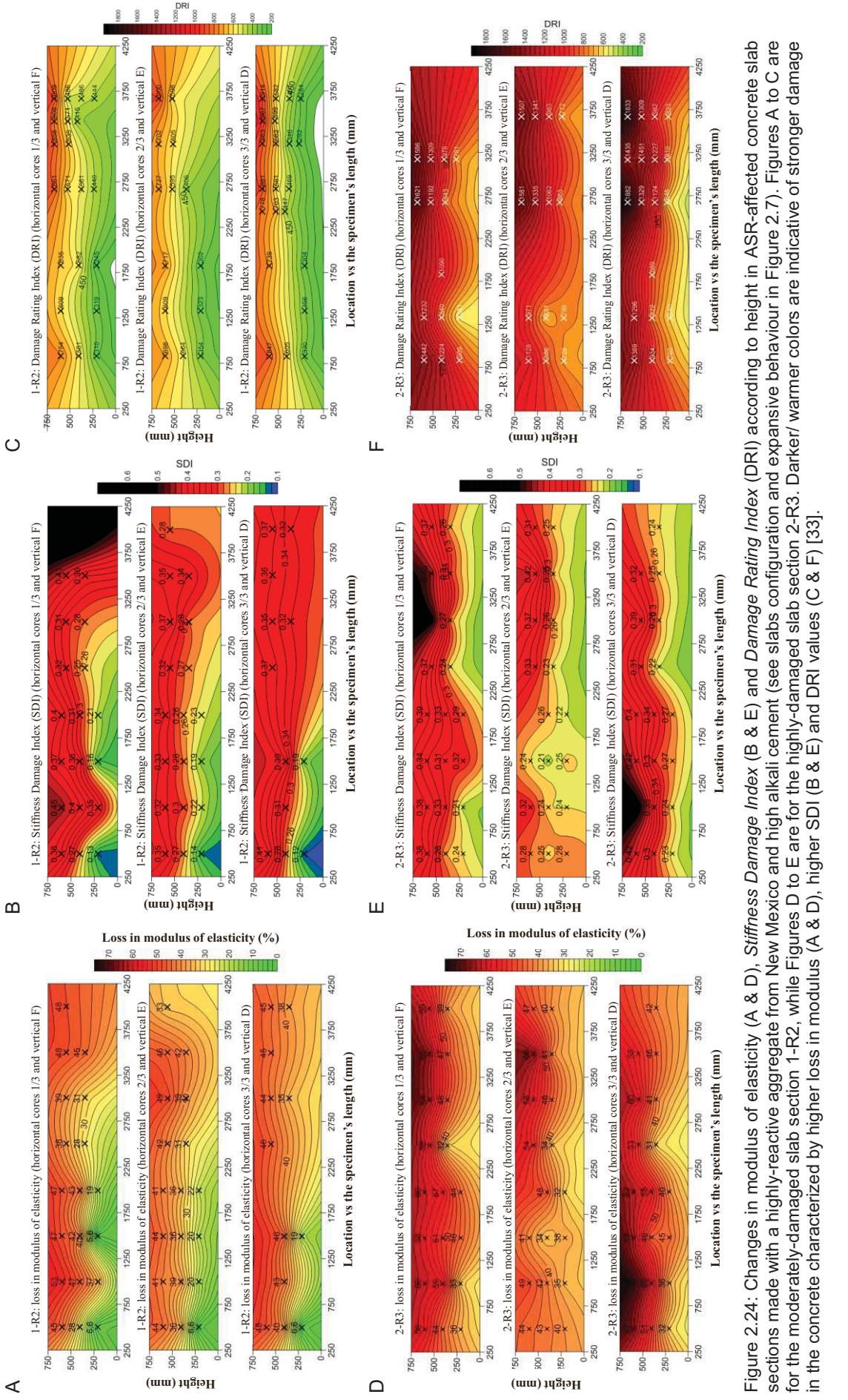

Figure 2.24: Changes in modulus of elasticity (A & D), *Stiffness Damage Index* (B & E) and *Damage Rating Index* (DRI) according to height in ASR-affected concrete slab sections made with a highly-reactive aggregate from New Mexico and high alkali cement (see slabs configuration and expansive behaviour in Figure 2.7). Figures A to C are for the moderately-damaged slab section 1-R2, while Figures D to E are for the highly-damaged slab section 2-R3. Darker/ warmer colors are indicative of stronger damage in the concrete characterized by higher loss in modulus (A & D), higher SDI (B & E) and DRI values (C & F) [33].

Figure 2.25: A. Bridge slab after sawing of a segment. B. Close-up view of strong horizontal cracking pattern on the section of a segment. [76].

The impact of coring location/orientation on the damage assessment in concrete affected by ASR is also highlighted from the testing of cores (100 mm in diameter) extracted from different elements of the Robert-Bourassa Charest overpass (Figure 2.16). Figure 2.26 presents the results of SDT (A) and DRI (B) testing carried out on cores taken from the footings, bridge deck and columns of the structure prior to its demolition in 2010/2011 [80]. In the case of the footings supporting the Y-shape columns (Figures 2.16A and 2.16H), the extent of ASR damage was determined on cores extracted from the exposed part of the foundation (e.g. Figure 2.16H) and from an apparently less damaged location protected from rain under the bridge deck. In addition, core sections were selected with care to perform evaluation of areas near the surface of the element and deeper inside (> 350 mm) [80] to assess the damage profile. In the case of the reinforced concrete columns, cores were extracted from highly exposed outer columns (Figures 2.16A and 2.16F) and inner columns protected from rain and solar radiations (Figure 2.16G). In the latter, the core sections were tested by removing the concrete cover (about 50 mm) and testing the concrete inside the reinforcement cage. Finally, in the case of the bridge deck, 100mm-diameter cores were obtained in the vertical, transverse and horizontal directions (Figure 2.16E) within the large cores (about 800 mm in diameter) extracted from the deck (Figures 2.16B and 2.16C). The core specimens were then recovered for testing in the top and bottom (i.e. close to the bottom reinforcing bars – Figure 2.16C) portions of the deck. The data illustrated in Figure 2.26 indicate the following [80]:

- higher damage (i.e. higher SDI and DRI values) was found in the exposed portion of the footing compared to the section protected under the bridge deck; also, the extent of damage was higher near the surface compared to the “core” of the element;
- higher damage was found in the bottom portion of the bridge deck, i.e. closer to the bottom reinforcement; this was common from the testing in the three directions of coring;
- the cores taken from the columns were showing the lowest damage level of all specimens tested, which is linked to the degree of confinement/reinforcement present in those members. There was no significant difference in the damage for the outer (exposed) and inner (non-exposed) columns.

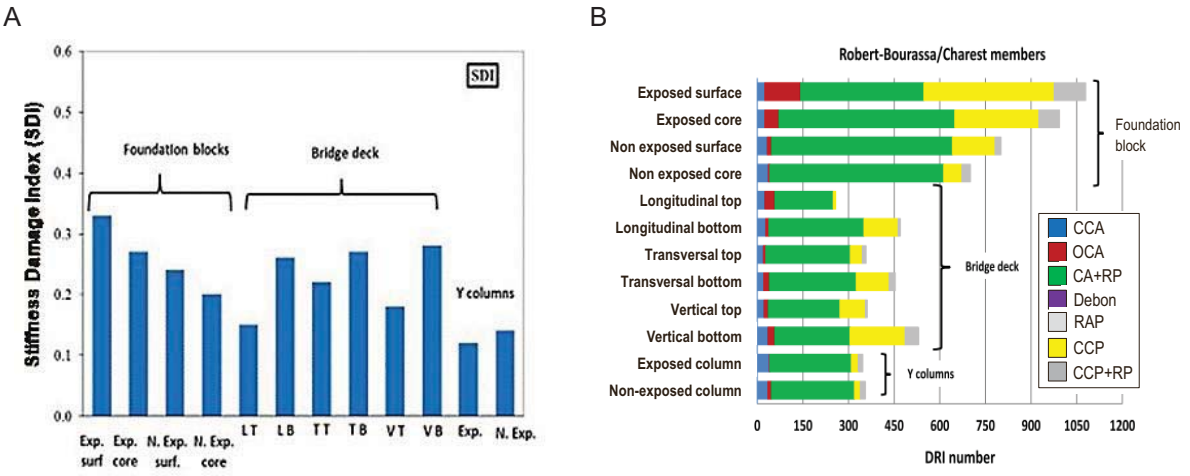

Figure 2.26: Results of testing of cores extracted from various structural elements of the Robert-Bourassa-Charest overpass. A. SDI results obtained from SDT testing. B. DRI results [80].

3. ALKALI-SILICA REACTION - CHEMICAL EFFECTS

The initiation, progress and extent of ASR is highly influenced by the external and internal chemical environments to which the aggregates/concrete are subjected. This chemical environment is highly impacted by the exposure/access to moisture, with numerous evidences coming from laboratory testing and field cases. The “alkali inventory” in concrete is also particularly critical. Portland cement is the main contributor of alkalis to the concrete pore solution, which correlate linearly with the OH^- concentration (or pH) [2]. Other sources of alkalis include SCMs (e.g., fly ash, slag, silica fume, natural pozzolans), chemical admixtures and aggregates. External sources such as seawater and deicing chemicals can also contribute to the concrete alkali content and to ASR [2]. In terms of potential reactivity, aggregates often respond differently to the concrete alkali content [1,81]; most aggregates generally show increased expansion with increasing concrete alkali content, although pessimum effects are possible. RILEM method AAR-10 [82] provides a procedure for the determination of the alkali threshold, for concrete mixtures incorporating or not SCMs, that will enable the safe use of reactive aggregates in concrete.

Bérubé et al. [83] used the HWE method to study the distribution of alkalis within/along cores extracted from mass concrete elements of several hydraulic structures. They found that the alkali concentration can vary significantly from the surface down into the bulk concrete, as affected by the particular environment to which the concrete elements are subjected under field conditions. Lower concentrations can result from alkali leaching by rain, runoff or “still” (reservoir of hydraulic dams) water, while local evaporation or migration can induce localized higher alkali concentrations. Plusquellec et al. [11] used the CWE method to study the “free alkali metal” profile in cores drilled from different locations in an ASR-affected dam in Norway, with different exposure conditions, i.e. permanently submerged, periodically submerged, atmospheric and sheltered. Polished slabs were also examined petrographically to quantify cracking density by Image Analysis (IA). The authors found that the concrete permanently or periodically submerged in water underwent alkali leaching in their first 100 mm. Leaching was also impacting the concrete section exposed to atmospheric conditions (wetting & drying cycles, rain), but to a lesser extent. Interestingly, the alkali metal profiles correlated relatively well with cracking density obtained by IA, with lower values being observed in the surficial zones suffering from alkali leaching.

One of the most critical question arising from investigations aiming at estimating the residual expansion of concrete affected by ASR is the alkali contribution from fine or coarse aggregates in concrete. Bérubé and Fournier [84] showed that large amounts of alkalis can be released from aggregates, the extent varying according to the test procedures used for extraction. RILEM AAR-08 [57] proposes a method for determining the potential long-term alkali contribution of alkalis from aggregates in field concrete. It consists in measuring the amounts of Na and K ions released from graded/ground ($<$ 4mm) aggregate particles immersed in KOH (0.7M) and NaOH (0.7M) solutions at 38 or 60°C. Although the development of such test procedures was an important step in the determination of potential alkali release from aggregates, a correlation with the actual contribution in field concretes remains to establish.

Figure 3.1 presents expansion curves for concrete cores, 150×300 mm in size, extracted in the vertical and horizontal directions from large concrete blocks made in the laboratory with a reactive metagreywacke coarse aggregate (GO) [85]. The testing was conducted as part of the same research program described in section 2.1.2 and involving mass concrete mixture (Essalik et al. [32]). For the purpose of the investigation, three different concrete alkali contents were used, i.e. 1.4 kg/m^3 (original alkali loading in the concrete dam), 3.0 and 4.6 kg/m^3. After about 550 days of expansion testing at 38°C and 100% RH, no expansive potential was noticed in the concrete with an alkali content similar to that of the original concrete mixture used in the dam (1.4 kg/m^3). Increasing expansion was however obtained with increasing concrete alkali content (3.0 and 4.6 kg/m^3) (Figure 3.1). Higher expansions were obtained for cores extracted in the vertical direction, i.e. in the direction of concrete pouring in the forms, which highlighted an anisotropic expansion behaviour for the test specimens. Such a behaviour has also been reported from other laboratory investigations [86,87]. HWE measurements conducted on concrete cores extracted from the dam revealed, despite significant variability, water soluble alkali contents (Na_2Oeq) ranging from 3.0 to 4.0 kg/m^3 in the concrete. Alkali contribution from the coarse and fine aggregates is suspected to be responsible for this important difference.

Another interesting field case comes from an on-going investigation conducted on an ASR-affected bridge structure crossing the St. Lawrence River in Montreal (Canada) (Figure 3.2). Testing of numerous core sections extracted from the footings of the piles (immersed in the river) confirmed that two types of concrete had been used at the time of construction. Concrete A was made with a manufactured limestone sand and a coarse aggregate consisting of a mixture of fine-grained reactive limestone and

non-reactive volcanic rock type; Concrete B was made with a reactive coarse limestone aggregate and a non-reactive natural (granitic) fine aggregate. Figure 3.3 highlights concrete compositions through micrographs of polished slab sections, including micro-XRF mapping. Extensive signs of ASR were found in both concrete types, but the extent of damage was significantly higher in the Concrete type B, as indicated by the DRI values obtained from a number of polished sections examined (Figure 3.4A). Interestingly, the water-soluble alkali content (HWE and CWE methods) measured on core specimens from the concrete footings revealed, despite significant variability in the test results, much higher water-soluble alkali contents in Concrete A (Figure 3.4B). This is thought to be related to the presence of the alkali-rich magmatic coarse aggregate in the latter. Gillott and Rogers [88] showed that the presence of an alkali-rich mineral (Dawsonite) in volcanic dykes in the Montreal area could be responsible for the release of alkalis when such rock types are used as concrete aggregates.

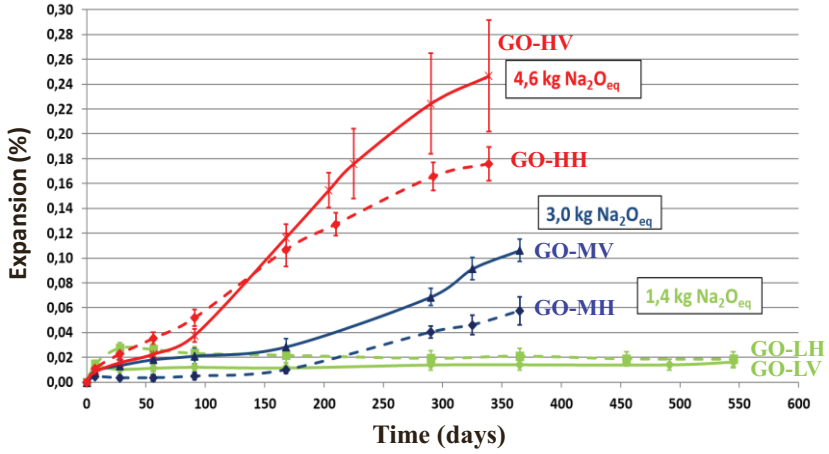

Figure 3.1: Evolution of the expansion of test specimens made from concrete mixtures incorporating the reactive GO metagreywacke aggregate. The specimens were obtained by coring in horizontal (H) and vertical (V) direction in large concrete blocks (high (H), Moderate (M) and low (L) alkali content). Error bars are given for the whole set of specimens, for a confidence level of 95% [85].

Figure 3.2: ASR-affected structure in the Montreal area (Canada).

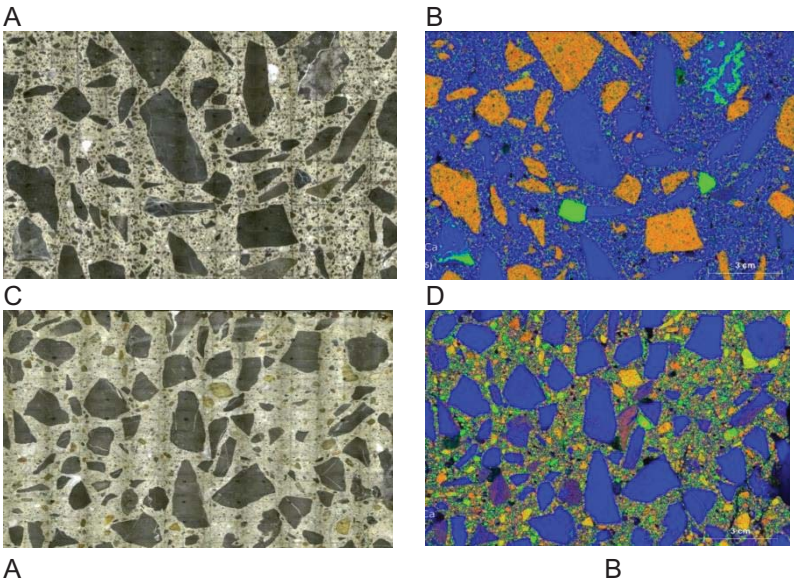

Figure 3.3: Polished core sections from the footings of concrete piles from an ASR-affected structure in Canada. Squares on slabs are 1 cm^2 in size. A & B. Type A concrete made of mixed coarse aggregate (limestone - blue - B) and magmatic rock - orange - B)); limestone fine aggregate (blue - B). C and D. Type B concrete made of limestone coarse aggregate (blue - D) and natural granitic-type sand (mixed colors – D). Colors are linked to chemical composition: blue – Ca, Si – green, Al – red. Ca is related to limestone particles, while silicate rocks (Si + Al) are associated to the magmatic rock particles (orange color in B). [89].

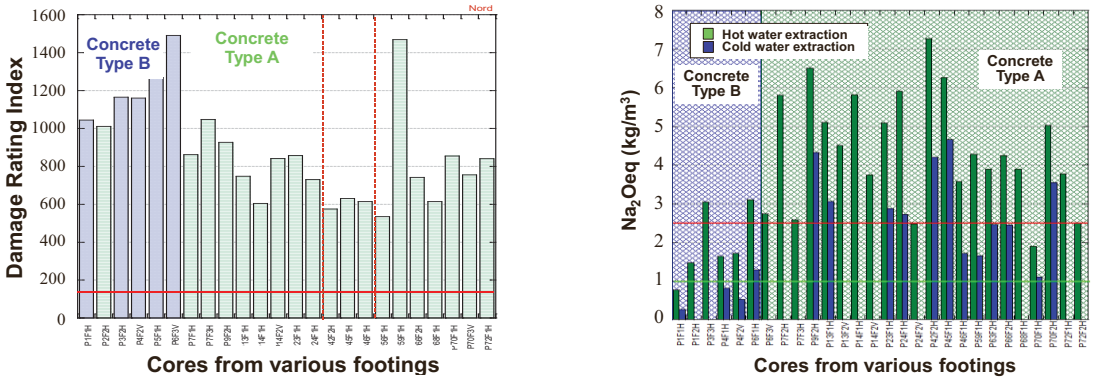

Figure 3.4: A. Results of Damage Rating Index determination on polished sections prepared from the concrete footings of several piles illustrated on Figure 3.2. The results are regrouped according to the two concrete compositions (A and B) identified in the polished sections. B. Results of the water-soluble alkali determination performed on concrete specimens from the footings of the piles illustrated on Figure A. Both hot water (HWE) and cold water (CWE) extraction methods were conducted on some of the concrete specimens for comparison purposes. Once again, the results are regrouped according to the two concrete compositions identified. [89].

4. CONCLUDING REMARKS

Despite extensive research conducted since the early 1940's, a lot of work remains to ensure a better understanding of the physical and chemical effects of ASR in concrete. Increasing efforts are spent in modeling the behavior of mortar and concrete specimens subjected to accelerated laboratory conditions in view of identifying key parameters responsible for the expansive behaviors of different reactive rock types and ultimately forecast their long-term performance in concrete structures under field conditions. Care should be exercised since accelerated testing often impact differently the behavior of various rock types depending on their composition (e.g. types of reactive silica) and textural characteristics, as well as the severity of the storage conditions (T°, RH, immersion in "salt" solution, etc.). Comparing the performance of various concrete specimens in both laboratory conditions and adequately monitored outdoor exposure sites (i.e. where environmental conditions can be closely monitored and their impact considered in the modelling process) will help validating and forecasting long-term field performance of various combinations of reactive rock types and cementitious materials.

The swelling properties of secondary products of ASR are known to vary according to their composition, texture, moisture access and location within the concrete specimens. Those products generate stresses within reacting aggregate particles and the surrounding cement paste that result in cracking patterns which may vary from one aggregate to another and on various mix properties. The coupling between ASR and the state of stress is complex. Although a reduction of the expansion is generally observed in the direction coinciding with that of the maximum compressive stress, the behavior observed in the other directions as well as the influence on the volumetric strains can vary greatly depending on the specific parameters of the study. Moreover, the level of stress required to fully mitigate ASR deformation in the maximum compressive stress direction also varies between studies. A better understanding is needed, notably by considering the physicochemical and mechanical effects at the microscale, as well as the interaction with the surrounding environment, in order to fully appreciate the resulting effects of ASR on the mechanical properties of concrete incorporating reactive aggregates.

Various tools exist for the condition assessment of concrete elements affected by ASR. The best approach still consists in combining non-destructive, physical, mechanical and petrographic characterization techniques, since the various concrete properties and characteristics show different levels of sensitivity to internal expansive reactions and their physical effects. For instance, the extent of cracking within the aggregate particles and cement paste, the presence of secondary reaction products within cracks, the orientation of cracking versus the applied stress, the location and direction of coring within structural members and with regards to the exposure conditions (especially the moisture access), the depth of the test specimen within the investigated element and the effective confinement provided by the reinforcement, etc. are all factors that will impact the condition assessments and should be carefully considered in interpreting the data and issuing recommendations.

The moisture and chemical environments within and around concrete elements have a strong impact on the development and progress of ASR. Alkali leaching, concentration, dilution, ingress, etc. directly impact the ASR reaction rate and cracking development and, in turn, the mechanical and structural

response of the concrete. One of the critical challenges in forecasting the future behavior of ASR-affected concrete remains the determination of the “alkali inventory” and especially potential alkali release from aggregates and other sources that may result in sustained reaction and related structural and durability implications.

5. ACKNOWLEDGMENTS

The authors would like to thank all students, technical assistants, research professionals, colleagues and collaborators from various funding agencies, private and public sector organizations for their help and support in the various projects at the source of the information/data presented in this paper.

6. REFERENCES

[1] Fournier B, Bérubé MA (2000) Alkali-aggregate reaction in concrete: A review of basic concepts and engineering implications. Canadian Journal of Civil Engineering, 27(2): 167-191.
[2] Thomas MDA, Fournier B, Folliard, KJ (2013) Alkali-Aggregate Reactivity (AAR) Fact Book. Federal Highway Administration (FHWA), U.S. Dept of Transportation, FHWA-HIF-13-019, 212p.
[3] Fournier B, Bérubé MA, Folliard KJ, Thomas MDA (2010) Report on the diagnosis, prognosis and mitigation of alkali-silica reaction (ASR) in transportation structures. Federal Highway Administration (FHWA), U.S. Dept of Transportation, FHWA-HIF-09-004, 154p.
[4] Sanchez LFM, Fournier B, Jolin M, Bastien J (2015) Evaluation of the Stiffness Damage Test (SDT) as a tool for assessing damage in concrete due to alkali-silica reaction (ASR): input parameters and variability of the test responses. Construction and Building Materials, 77: 20-32.
[5] Sanchez LFM, Fournier B, Jolin M, Bastien J, Mitchell D (2016) Practical use of the Stiffness Damage Test (SDT) for assessing damage in concrete infrastructure affected by alkali-silica reaction. Construction and Building Materials, 125: 1178-1188.
[6] Villeneuve V, Fournier B (2012) Determination of the damage in concrete affected by ASR — the Damage Rating Index (DRI). Proc. of the 14th Int. Conf. on AAR in concrete, Austin (Texas).
[7] Champagne M (2020) Applying the Damage Rating Index for the spatial damage assessment in concrete specimens affected by ASR. MSc memoir, Université Laval (Québec, Canada).
[8] Roy-Tremblay M (2022) Utilisation de l’analyse d’images comme outil de quantification de l’endommagement des bétons atteints de RAS. Mémoire de M.Sc., U. Laval (Québec, Canada).
[9] LCPC (1997) Détermination de l’indice de fissuration d’un parement de béton. Méthode d’essai No 47, Laboratoire Central des Ponts et Chaussées, Paris (France).
[10] Bérubé MA, Frenette J, Rivest M, Vézina D (2002) Measurement of the alkali content of concrete using hot water extraction. Cement, Concrete and Aggregates, 24(1): 28-36.
[11] Plusquellec G, Geiker MR, Lindgård J, DeWeerdt K (2018) Determining the free alkali metal content in concrete – Case study of an ASR-affected dam, Cement and Concrete Research, 105: 111-125.
[12] Pedneault A (1996) Développement de procédures d’essai et d’analyse pour l’évaluation du potentiel résiduel de réaction, d’expansion et de détérioration du béton affecté de RAS. Mémoire de M.Sc., U. Laval, 132 p.
[13] Olajide O, Nokken M, Sanchez LFM (2022) A review on the role of moisture and temperature in ASR. Proc. of the 16th Int. Conf. on AAR in concrete, Lisbon (Portugal).
[14] Lindgård J, Thomas MD, Sellevold EJ, Pederson B, Andiç-Cakir O, Justnes H, Ronning TF (2013) ASR-performance testing: Influence of specimen pre-treatment, exposure conditions and prism size on alkali leaching and prism expansion. Cement and Concrete Research, 53: 68-90.
[15] Gao XX, Multon S, Cyr M, Sellier A (2012) Contribution to the requalification of ASR damaged structures: Assessment of the ASR advancement in aggregates. Proc. of the 14th Int. Conf. on AAR in concrete, Austin (USA).
[16] Béland F (2020) Détermination de l’influence des paramètres physico-chimiques de base du béton sur la cinétique et le potentiel résiduel de RAS. Mémoire de M.Sc., U. Laval, Québec (Canada).
[17] Claude J (2020) Évaluation de la cinétique et du potentiel résiduel de la réaction alcalis-silice (RAS) dans les bétons affectés. Mémoire de M.Sc., U. Laval, Québec (Canada).
[18] Fournier B, Lindgård J, Wigum BJ, Borchers I (2018) Outdoor exposure site testing for preventing Alkali-Aggregate Reactivity in concrete – a review. International Conference on Concrete Repair, Rehabilitation and Retrofitting. Cape Town (South Africa).
[19] Lu D, Fournier B, Grattan-Bellew PE (2006) Effect of aggregate particle size on determining alkali-silica reactivity by accelerated tests. Journal of ASTM International, 3 (9).

[20] CSA A23.2-27A (2019) Standard practice to identify degree of alkali-reactivity of aggregates and to identify measures to avoid deleterious expansion in concrete, CSA A23.2-19 – test methods and standard practices for concrete. CSA, Mississauga, Ontario, Canada, 594-610.
[21] Medeiros S, Fernandes I, Fournier B, Nunes JC, Santos Silva A, Ramos V, Soares D (2022) Alkali-silica reaction in volcanic rocks: a worldwide comparative approach. Accepted for publication in Materiales de Construcción (2022).
[22] Fournier B, Bérubé MA (2000) Alkali-aggregate reaction in concrete: A review of basic concepts and engineering implications. Canadian Journal of Civil Engineering, 27(2): 167-191.
[23] Fournier B, Chevrier R, Bilodeau A, Nkinamubanzi PC, Bouzoubaa N (2016) Comparative field and laboratory investigations on the use of supplementary cementing materials (SCMs) to control ASR in concrete. Proc. of the 15th Int. Conf. on AAR in concrete, Sao Paulo (Brazil).
[24] Fournier B, Chevrier R, DeGrosbois M, Lisella R, Folliard KJ, Ideker J, Shehata M, Thomas MDA, Baxter S (2004) The accelerated concrete prism test (60°C) : variability of the test method and proposed expansion limits. Proc. of the 12th Int. Conf. on AAR in concrete, Beijing (China), Beijing World Publishing Corp., 1: 314-323.
[25] Naranjo-Salazar F (2022) Évaluation de l'efficacité d'un ajout cimentaire alternatif (aluminosilicate) pour contrecarrer la RAS dans le béton. Mémoire de M.Sc., U. Laval, Québec (Canada).
[26] Le Roux A, Massieu E, Godart B (1992) Evolution under stress of a concrete affected by AAR - application to the feasilbility of strengthening a bridge by prestressing. Proc. of the 9th Int. Conf. on AAR in concrete, London (UK), Volume 2.
[27] Larive C (1997) Apports combinés de l'expérimentation et de la modélisation à la compréhension de l'alcali-réaction et de ses effects mécaniques. Thèse de doctorat, LCPC (Paris), 327 p.
[28] Multon S, Toutlemonde F (2006) Effect of applied stress on alkali-silica reaction - induced expansions. Cement and Concrete Research, 36: 912-920.
[29] Liaudat J, Carol IM, Lopez C, Saouma, V (2018) ASR expansions in concrete under triaxial confinement. Cement and Concrete Research, 86: 160–170.
[30] Gautam BP, Panesar DK, Sheikh SA, Vecchio FJ (2017) Multiaxial Expansion-Stress Relationship for ASR-Affected Concrete. ACI Materials Journal, 114-M17: 171-184.
[31] Dunant CF, Scrivener K (2012) Effects of uniaxial stress on alkali–silica reaction induced expansion of concrete. Cement and Concrete Research, 42: 567-576
[32] Essalik S, Bissonnette B, Fournier B, Multon S (2022) Influence des conditions mécaniques et hygrométriques sur le comportement volumétrique d'un béton de masse affecté par la RAS. Conférence Internationale Francophone NoMaD, Montpellier (France), November 2022.
[33] Allard A, Bilodeau S, Pissot F, Bastien J, Fournier B (2016) Étude du comportement de dalles épaisses atteintes de RAS. Projet réalisé pour le compte du ministère des transports du Québec (Projet R651). Dépt. de génie civil et de génie des eaux, Université Laval. Rapport final, 508p.
[34] Allard A, Bilodeau S, Pissot F, Fournier B, Bastien J, Bissonnette B (2016) Performance evaluation of thick concrete slabs affected by ASR: Part I: Materials aspects. Proc. of the 15th Int. Conf. on AAR in concrete, Sao Paulo (Brazil).
[35] Allard A, Bilodeau S, Pissot F, Fournier B,. Bastien J, Bissonnette B (2018). Expansive behavior of thick concrete slabs affected by ASR. Construction and Building Materials, 171: 421-436.
[36] Ministry of Transportation of Ontario (MTO) database on Kingston Exposure site. 2021.
[37] Hooton RD, Rogers CA, MacDonald CA, Ramlochan T (2013) Twenty-Year Field Evaluation of Alkali-Silica Reaction Mitigation. ACI Materials Journal, 110 (5): 539-548.
[38] Barbotin-Albinski S, Shi Z., Boehm-Courjault E, Leemann A, Scrivener K (2022). Characterization of synthetic ASR products by TEM and preliminary comparison with on-field early stage products, Proc. of the 16th Int. Conf. on AAR in concrete, Lisbon (Portugal).
[39] Leemann A, Fernandes I, Katayama T, Broekmans MATM (2016) Types of alkali-aggregate reactions and the products formed. Proceedings of the Institution of Civil Engineers: Construction Materials, 169 (CM3): 128-135.
[40] Urhan S (1987) Alkali silica and pozzolanic reactions in concrete. Part 1: Interpretation of published results and a hypothesis concerning the mechanism. Cement & Concrete Research, 17: 141-152.
[41] Zhang C, Sorelli L, Fournier B, Duchesne J, Bastien J, Chen Z (2017) Stress-relaxation of crystalline alkali-silica reaction products: Characterization by micro- and nanoindentation and simplified modeling. Construction and Building Materials, 148: 455–464.
[42] Gholizadeh-Vayghan A, Rajabipour F, Khaghani M, Hillman M (2019) Characterization of viscoelastic behavior of synthetic ASR gels. Cement and Concrete Composites, 104: 103359.

[43] Morenon P (2017) Modélisation des réactions de gonflement interne des bétons avec prise en compte des couplages poro-mécaniques et chimiques. Doctoral thesis, Université Toulouse 3 Paul Sabatier, 256 p.
[44] Neville AM (1995) Properties of concrete (Vol. 5): Pearson London.
[45] Troxell G E, Raphael JM, Davis RE (1958) Long-time creep and shrinkage tests of plain and reinforced concrete, Proc. ASTM., 58: 1101–1120.
[46] Giorla AB, Scrivener KL, Dunant CF (2015) Influence of visco-elasticity on the stress development induced by alkali-silica reaction. Cement and Concrete Research, 70 : 1-8.
[47] Bérard J, Roux R (1986) La viabilité des bétons du Québec: le rôle des granulats. Canadian Journal of Civil Engineering, 13 (1): 12–24.
[48] Guédon-Dubied JS, Cadoret G, Durieux V, Martineau F, Fasseu P, Van Overbecke V (2000). Study on Tournai limestone in Antoing Cimescaut quarry — petrological, chemical and alkali-reactivity approach, Proc. of the 11th Int. Conf. on AAR in concrete, Quebec (Canada), 335–344.
[49] Fournier B, Fecteau PL, Villeneuve V, Tremblay S, Sanchez LFM (2015) Description of petrographic features of damage in concrete used in the determination of the Damage Rating Index (DRI) – A petrographic Album. Université Laval, Quebec City (Canada), 59p.
[50] Dunant CF, Scrivener KL (2009) Micro mechanical modeling of ASR induced degradation using the AMIE framework, Cement and Concrete Research 40: 517–525.
[51] Dunant CF, Bentz E (2012) The effect of multi-axial restraint on ASR-affected concrete, Proc. of the 14th Int. Conf. on AAR in concrete, Austin (Texas).
[52] Reinhard HW, Mielich O (2011) A fracture mechanics approach to the crack formation in alkali sensitive grains. Cement and Concrete Research, 41 : 255- 262.
[53] Sanchez LFM, Fournier B, Jolin M, Duchesne J (2015) Reliable quantification of AAR damage through assessment of the Damage Rating Index (DRI). Cement & Concrete Research, 67: 74-92.
[54] Bustamante-Bedoya MA (2015) Évaluation de l'état d'endommagement du béton atteint de réaction alcalis-silice à l'aide de l'analyse d'images. Mémoire de M.Sc, U. Laval (Québec, Canada).
[55] Lindgård J, Haugen M, Castro N, Thomas, MDA (2012) Advantages of using plane polished section analysis as part of microstructural analysis to describe internal cracking due to alkali-silica reactions. Proc. of the 14th Int. Conf. on AAR in concrete, Austin (Texas).
[56] Lindgård J (2016) Results from ASR performance testing initiated within COIN WP2 – Follow-up study. SINTEF report for Project no. 102000442-7, 83p.
[57] Menéndez E, Santos Silva A, Duchesne J (2021) Recommendation of RILEM TC 258-AAA: RILEM AAR-8: determination of potential releasable alkalis by aggregates in concrete. Materials and Structures 54: 205.
[58] Champagne M, Lindgård J, Fournier B, Bissonnette B (2022) Applying the Damage Rating Index for the spatial damage assessment in concrete specimens affected by alkali-silica reaction. Proc. of the 16th Int. Conf. on AAR in concrete, Lisbon (Portugal).
[59] Champagne M, Pedersen B, Rodum E, Lindgard J, Fournier B, Bissonnette B (2022) Field and laboratory investigations for the condition assessment of ASR-affected structures. Ph.D. Thesis in evaluation. Laval University (Québec, Canada).
[60] Figg J (1986) ASR – Inside phenomena and outside effects (crack origin and pattern). Proc. of the 7th Int. Conf. on AAR in concrete, Ottawa (Canada). Noyes Publication (USA).
[61] Allard A, Fournier B, Bastien J, Bissonnette B, Sanchez LFM, Duchesne J (2016) Evaluation of the degree of damage caused by ASR in a highway pavement : a case study. Proc. of the 15th Int. Conf. on AAR in concrete, Sao Paulo (Brazil).
[62] Thomas MDA, Fournier B, Folliard KJ, Resendez B (2011) ASR – Surveying and tracking guidelines. Federal Highway Administration (FHWA), FHWA-HIF-12-046, 35p.
[63] Stark D, Depuy G (1987) Alkali-Silica Reaction in Five Dams in Southwestern United States. Proc. of the Katherine and Bryant Mather International Conf. on Concrete Durability, Atlanta, Georgia (USA), April 1987, ACI SP-100: 1759-1786.
[64] Courtier RH (1990) The Assessment of ASR-Affected Structures. Cement and Concrete Composites, 12: 191-201.
[65] Bérubé MA, Chouinard D, Pigeon M, Frenette J, Rivest M, Vézina D (2002) Effectiveness of sealers in counteracting alkali-silica reaction in highway median barriers exposed to wetting and drying, freezing and thawing, and deicing salt, Canadian Journal of Civil Engineering. 29: 329–337.
[66] Champagne M, Roy-Tremblay M, Fournier B, Duchesne J, Bissonnette B (2019) Long-term effectiveness of sealers in counteracting alkali–silica reaction in highway median barriers exposed to wetting and drying, freezing and thawing,and de-icing salts. 17th Euroseminar on Microscopy Applied to Building Materials (EMABM), University of Toronto, Toronto, Canada, May 20-23, 6p.

[67] Blight GE, McIver JR, Schutte WK, Rimmer R (1981) The effects of alkali-aggregate reaction on reinforced concrete structures made with Witwatersrand quartzite aggregate. Proc. of the 5th Int. Conf. on AAR in concrete, Cape Town (South Africa), paper S252/15.
[68] Swamy RN, Al-Asali MM (1986) Influence of ASR on the Engineering Properties of Concrete. (Ed. V.H. Dodson), ASTM STP 930, American Society for Testing and Materials, 69-86.
[69] Clayton N (1989) Structural Performance of ASR Affected Concrete. Proc. of the 8th Int. Conf. on AAR in concrete, Kyoto (Japan), 671-676.
[70] Siemes T, Visser J (2000) Low Tensile Strength in Older Concrete Structures with ASR. Proc. of the 11th Int. Conf. on AAR in concrete, Quebec City (Canada), 1029-1038.
[71] Smaoui N, Bissonnette B, Bérubé MA, Fournier B, Durand B (2006) Mechanical properties of ASR-affected concrete containing fine or coarse reactive aggregates. Journal of ASTM International 3(2).
[72] Sanchez LFM, Fournier B, Jolin M, Mitchell D, Bastien J (2017). Overall assessment of Alkali-Aggregate Reaction (AAR) in concretes presenting different strengths and incorporating a wide range of reactive aggregate types and natures. Cement and Concrete Research, 93: 17-31.
[73] Hobbs DW (1986) Alkali-Silica Reaction in Concrete. The Structural Engineer, 64A(12): 381-383.
[74] Kubo Y, Nakata M (2012) Effect of reactive aggregate on mechanical properties of concrete affected by ASR. Proc. of the 14th Int. Conf. on AAR in concrete. Austin (Texas).
[75] Giaccio G, Zerbino R, Ponce JM, Batic R (2008). Mechanical behavior of concretes damage due to ASR. Cement and Concrete Research. 38: 993-1004.
[76] Barbosa RA, Hansen SG, Hansen KK, Hoang LC (2018) Influence of alkali-silica reaction and crack orientation on the uniaxial compressive strength of concrete cores from slab bridges. Construction and Building Materials, 176: 440-451.
[77] Gautam BP (2016) Multiaxially Loaded Concrete Undergoing Alkali-Silica Reaction (ASR). Thèse de doctorat, Université de Toronto, 187 p.
[78] Zahedi A, Trottier C, Sanchez LFM, Noël M (2021) Microscopic assessment of ASR-affected concrete under confinement conditions. Cement and Concrete Research, 145: 106456.
[79] Zahedi A, Trottier C, Sanchez LFM, Noël M (2022) Evaluation of the induced mechanical deterioration of alkali-silica reaction affected concrete under distinct confinement conditions through the Stiffness Damage Test, Cement and Concrete Composites, 126: 104343.
[80] Sanchez LFM, Fournier B, Mitchell D, Bastien J (2020) Condition assessment of an ASR-affected overpass after nearly 50 years in service. Construction and Building Materials, 236: 117554.
[81] Rogers CA, Grattan-Bellew PE, Hooton RD, Ryell J, Thomas MDA (2000) Alkali-aggregate reactions in Ontario. Canadian Journal of Civil Engineering, 27(2): 246-260.
[82] Ronning TJ, Wigum BJ, Lindgard J (2021) Recommendation of RILEM TC 258-AAA: RILEM AAR-10: Determination of binder combinations for non-reactive mix design using concrete prisms–38°C test method. Materials and Structures, 54:204, 30p.
[83] Bérubé MA, Dorion JF, Rivest M (2000) Distribution of alkalies in concrete structures affected by alkali-silica reactivity and contribution by aggregates. Proc. of the 11th Int. Conf. on AAR in concrete, Quebec City (Canada), 139-148.
[84] Bérubé MA, Fournier B (2004) Alkalis releasable by aggregates in concrete – significance and test methods. Proc. of the 14th Int. Conf. on AAR in concrete. Beijing (China): volume I.
[85] Darveau JB (2021) Contribution à l'étude du comportement d'un béton de masse affecté par la réaction alcalis-silice : évolution et anisotropie de l'expansion, de l'endommagement et des propriétés mécaniques. Mémoire de M.Sc., Université Laval, Québec (Canada).
[86] Smaoui N, Bérubé MA, Fournier B, Bissonnette B (2004) Influence of Specimen Geometry, Orientation of Casting Plane, and Mode of Concrete Consolidation on Expansion Due to ASR. Cement, Concrete and Aggregates, 26(2): 1-13.
[87] Villemure FA, Fiset M, Bastien J, Mitchell D, Fournier B (2019) Behavior of Epoxy Bonded Bars in Concrete Affected by Alkali-Silica Reaction. ACI Materials Journal, 116 (6): 14p.
[88] Gillott JE, Rogers CA (1994) Alkali-aggregate reaction release of alkalis. Magazine of Concrete Research 46 (167): 99-112.
[89] Thériault N (2022) Quantification actuelle et projection de l'endommagement potentiel par la réaction alcalis-silice (RAS) d'une structure de béton en conditions immergées. Mémoire de M.Sc. (en préparation), U. Laval, Québec (Canada).